Acta Geologica Sinica (English Edition), 2019, 93(5): 1188–1204

Chronological Constraints on Late Paleozoic Collision in the Southwest Tianshan Orogenic Belt, China: Evidence from the Baleigong Granites

HUO Hailong[1, 2], CHEN Zhengle[1, 2, 3, *], ZHANG Qing[1, 2], HAN Fengbin[1, 2, 4], ZHANG Wengao[1, 2], SUN Yue[3], YANG Bin[3] and TANG Yanwen[5]

[1] *Laboratory of Dynamic Diagenesis and Metallogenesis, Institute of Geomechanics, Chinese Academy of Geological Sciences, Beijing 100081, China*
[2] *Key Laboratory of Paleomagnetism and Tectonic Reconstruct, Ministry of Natural Resources, Beijing 100081, China*
[3] *Faculty of Earth Sciences, East China University of Technology, Nanchang 330013, China*
[4] *College of Earth and Planetary Sciences, University of Chinese Academy of Sciences, Beijing 100049, China*
[5] *Institute of Geochemistry, Chinese Academy of Sciences, Guiyang 550081, China*

Abstract: The Baleigong granites, located in the western part of the southwestern Tianshan Orogen (Kokshanyan region, China), records late Paleozoic magmatism during the late stages of convergence between the Tarim Block and the Central Tianshan Arc Terrane. We performed a detailed geochronological and geochemical study of the Baleigong granites to better constrain the nature of collisional processes in the Southwest Tianshan Orogen. The LA-ICP-MS U-Pb zircon isotopic analyses indicate that magmatism commenced in the early Permian (~282 Ma). The granite samples, which are characterized by high contents of SiO_2 (67.68–69.77 wt%) and Al_2O_3 (13.93–14.76 wt%), are alkali-rich and Mg-poor, corresponding to the high-K calc-alkaline series. The aluminum saturation index (A/CNK) ranges from 0.93 to 1.02, indicating a metaluminous to slightly peraluminous composition. Trace element geochemistry shows depletions in Nb, Ta, and Ti, a moderately negative Eu anomaly (δEu=0.40–0.56), enrichment in LREE, and depletion in HREE ($(La/Yb)_N$=7.46–11.78). These geochemical signatures are characteristic of an I-type granite generated from partial melting of a magmatic arc. The I-type nature of the Baleigong granites is also supported by the main mafic minerals being Fe-rich calcic hornblende and biotite. We suggest that the high-K, calc-alkaline I-type granitic magmatism was generated by partial melting of the continental crust, possibly triggered by underplating by basaltic magma. These conditions were likely achieved in a collisional tectonic setting, thus supporting the suggestion that closure of the South Tianshan Ocean was completed prior to the Permian and was followed (in the late Paleozoic) by collision between the Tarim Block and the Central Tianshan Arc Terrane.

Key words: I-type granite, Late Paleozoic, zircon U–Pb dating, Baleigong granites, Southwest Tianshan

Citation: Huo et al., 2019. Chronological Constraints on Late Paleozoic Collision in the Southwest Tianshan Orogenic Belt, China: Evidence from the Baleigong Granites. Acta Geologica Sinica (English Edition), 93(5): 1188–1204. DOI: 10.1111/1755-6724.14353

1 Introduction

The Central Asian Orogenic Belt (CAOB) is one of the largest accretionary orogenic systems in the world, situated between the Siberian Craton to the north and the Tarim and North China Cratons to the south (Şengör et al., 1993; Jahn et al., 2000; Kröner et al., 2007; Windley et al., 2007; Xiao et al., 2008, 2013; Xiao and Santosh, 2014). The CAOB experienced a long history of orogenesis and records evidence of accretionary orogenesis and continental growth during the Phanerozoic (Cai et al., 2010; Gao et al., 1998, 2009a, b, 2011; Han et al., 2010, 2011, 2015, 2016; Long et al., 2007; Xiao et al., 2008; Xiao et al., 2013; Xiao and Santosh, 2014; Long and Huang, 2017). The Southwest Tianshan Orogenic Belt (STOB) in China is located in the southwestern part of the CAOB (Fig. 1). This orogen records the late Paleozoic final amalgamation of the Siberian Craton and Tarim Craton (Jahn et al., 2000; Windley et al., 2007; Glorie et al., 2012, 2015; Kröner et al., 2007, 2014; Xiao et al., 2013; Xiao and Santosh, 2014; Klemd et al., 2014, 2015; Chen et al., 2018). As such, studying the tectonic evolution of the Southwest Tianshan can improve Phanerozoic reconstructions of Eurasia (Xiao et al., 2008). However, the tectonic history of the STOB is controversial, due in part to a lack of field geological data and high-resolution geochronological data. In particular, the timing of the late Paleozoic closing of the South Tianshan Ocean and the subsequent collisional orogenesis are debated, with previous suggestions including Late Devonian (Charvet Jacques et al., 2011), early Carboniferous (Xia et al., 2002; Shu et al., 2007; Gao et al., 2009b), late Carboniferous to early Permian (Hao and Liu , 1993; Liu et al., 1996; Kang et al., 2011), and Triassic (Zhang et al., 2005; Li et al., 2009).

* Corresponding author. E-mail: chenzhengle@263.net

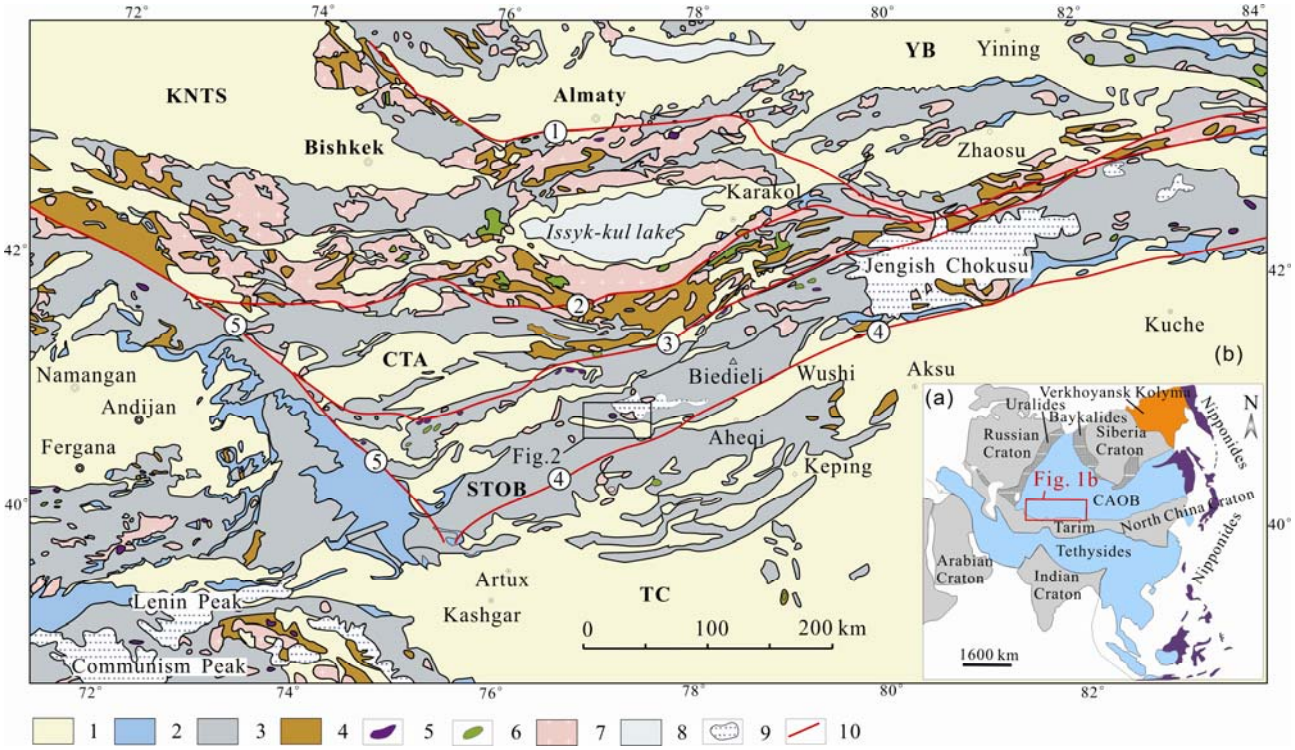

Fig. 1. (a) Tectonic map of the Central Asian Orogenic Belt (CAOB) (after Şengör et al., 1993; Chen et al., 2018). (b) Simplified geological map of the Chinese Southwest Tianshan Orogen and adjacent regions (after Gao et al., 2009a; Klemd et al., 2015).
1, Cenozoic strata; 2, Mesozoic strata; 3, Paleozoic strata; 4, Precambrian strata; 5, ophiolitic mélange; 6, ultramafic–mafic intrusion; 7, granite; 8, lake; 9, glacier; 10, fault; ①: Djalair–Naiman Suture; ②: Nikolaev Line–North Nalati Suture; ③: South Central Tianshan Suture; ④: North Tarim Fault; ⑤: Talas–Fergan Fault; KNTS–Kazakhstan Northern Tianshan; YB–Yili Block; TC–Tarim Craton; CTA–Central Tianshan Arc Terrane; STOB–Southwest Tianshan Orogenic Belt.

In this study, we present petrographic, geochemical, and geochronological data of 12 samples from the Baleigong granites (Fig. 1b), including the results of electron microprobe, zircon LA-ICP-MS, and whole-rock geochemical analyses. The results, together with existing data, provide information on the properties of the Baleigong granites and further constrain the timing of collisional orogenesis following the closure of the Southern Tianshan Ocean.

2 Geological Background

The Southwest Tianshan Orogenic Belt and adjacent areas can be subdivided into the Kazakhstan-Yili Block (KYB), the Northern Tianshan (NTS), the Central Tianshan Arc Terrane (CTA), and the Southwest Tianshan Orogenic Belt (STOB) (Gao et al., 2006, 2009b; Jiang et al., 2014; Klemd et al., 2014, 2015). This subdivision is broadly based on the distinctive tectonic suture zones (i.e. the Djalair–Naiman Suture, the Nikolaev Line–North Nalati Suture, the South Central Tianshan Suture, the North Tarim Fault and the Talas–Fergan Fault (Fig. 1b). The extensive South Tianshan Orogenic Belt is interpreted as a late Paleozoic collisional belt located between the Middle Tianshan and the Tarim Block (Windley et al., 1990; Gao et al., 1998; Yin et al., 1998; Xiao et al., 2000; He et al., 2001; Chen et al., 2002; Glorie et al., 2011; Brunet et al., 2017). The Southwest Tianshan Orogenic Belt is composed mainly of Cambrian–Carboniferous marine carbonates, clastic rocks, cherts and interlayered volcanics, ophiolite mélange, Mesozoic–Cenozoic continental clastic rocks, and Hercynian intrusive rocks (Allen et al., 1992; Carroll et al., 1995; Chen et al., 2002; Zhang et al., 2005; Gao Jun et al., 2006, 2009; Xiao et al., 2013; Jiang et al., 2014; Han et al., 2015; Klemd et al., 2015; Gou et al., 2016). The Silurian-Carboniferous marine sedimentary (i.e., Late Devonian–Early Carboniferous thick carbonate platforms) and volcanic rocks constitute the main part of the strata in the Southwest Tianshan Orogenic Belt (Gao et al, 1995, 1998; Xiao et al., 2013; Brunet et al., 2017). A HP-UHP metamorphic belt, composed of eclogites, blueschists and greenschists, is exposed along the northernmost of the Southwest Tianshan Orogenic Belt (Gao, 1997; Gao et al., 2000, 2011; Li et al., 2016). The HP-UHP metamorphism was formed by continuing oceanic–continental subduction of South Tianshan Ocean beneath Tarim Block in the late Paleozoic (Li et al., 2016).

The Baleigong granites are located in the western part of the Southwest Tianshan Orogenic Belt (Fig. 1b), intruding sedimentary rocks of the Wupata'erkan Group (Fig. 2). The strata exposed in the Baleigong area include the middle Devonian Tuogemaiti Formation, Devonian-Carboniferous Wupata'erkan Group, Earty Carboniferous Aiketike Group and Carboniferous Kalazhierjia Formation (from oldest to youngest). The Wupata'erkan Group is characterized by thick carbonate sequences, interlayered chert, mudstone, volcanic rocks, and ophiolite mélange,

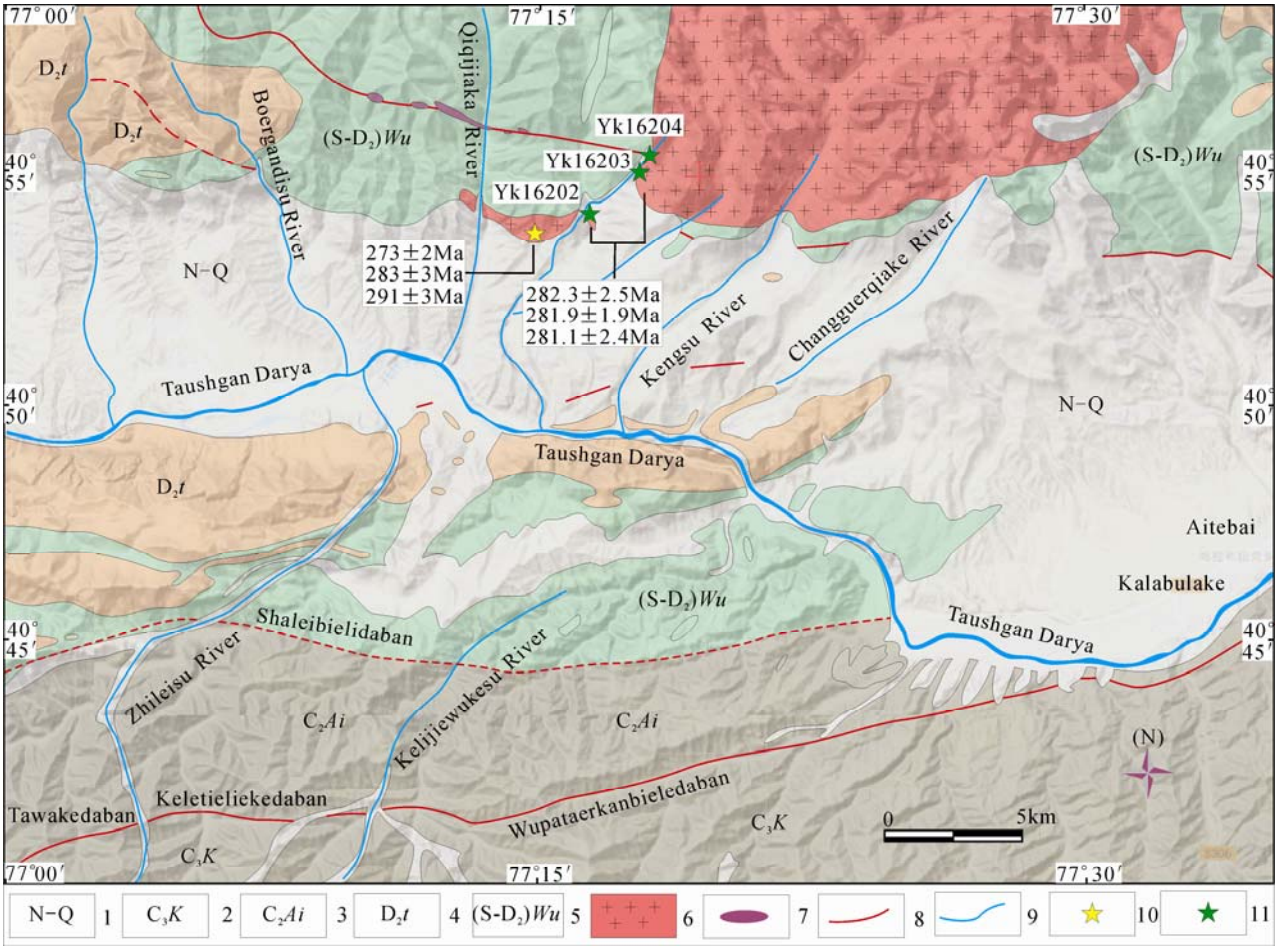

Fig. 2. Geological map of the Baleigong area (after Wang et al., 2007a) showing sampling sites.
1, Cenozoic strata; 2, Kangkelin Group; 3, Aiketike Group; 4, Tuoshigan Formation; 5, Wupataerkan Group; 6, Baleigong Granite; 7, ultramafic–mafic intrusion; 8, fault; 9, river; 10, sampling site (previous study; Wang et al., 2007a; Huang et al., 2015); 11, sampling site (this study).

which have locally experienced low-grade greenschist facies metamorphism (Wang et al., 2007a, b; Wang et al., 2008; Kang et al., 2011; Li et al., 2009; Wang et al., 2012). The SHRIMP U-Pb zircon data of the basalt from the Baleigong ophiolite mélange (also named Qiqijianake ophiolite mélange) formed in the Early Devonian (399 Ma; Wang et al., 2012). The physical features of the radiolarian fossils in the cherts indicate that the Wupata'erkan Group formed during the Late Devonian-Early Carboniferous (Li et al., 2009; Kang et al., 2011). The geochemical characteristics of the cherts in the Wupata'erkan Group indicate the cherts formed in a residual sea environment during the early Carboniferous (Kang et al., 2011).

The Baleigong granite is composed mainly of granodiorite and granite. The geochronology and geochemistry of the Baleigong Pluton have been extensively studied on a small apophysis at the edge of the pluton (Wang et al., 2007a; Liu et al., 2013; Huang et al., 2015). Wang et al. (2007a) suggested that the zircon crystallization ages of the granite is 273±2 Ma in the Baleigong pluton, indicate a Guadalupian (Permian) magmatic event in the Baleigong area (Fig. 2). Huang et al. (2015) reported the 291±3 Ma and 283±3 Ma for the biotite monzogranite of the Baleigong pluton (Fig. 2). But the magmatism and the genesis of the main pluton remains uncertain (Wang et al., 2007a; Liu et al., 2013; Huang et al., 2015). Some authors have suggested that high-K granitic magmatism was associated with post-orogenic collapse or the transition between collision and post-collision stages (Wang et al., 2007a). Others proposed that the Baleigong granite is an A-type granite that acted as a 'stitching pluton' (Zhang et al., 2009; Liu et al., 2013; Huang et al., 2015).

3 Sampling and Analytical Methods

3.1 Sampling and description

This study collected samples from the following areas: (1) the main body of the pluton (Yk16204) (Fig. 2 and Fig. 3a–b); (2) the small apophysis at the edge of the Baleigong Granites (sample Yk16202) (Fig. 3c); and (3) a granite porphyry that intruded the Wupata'erkan Group (Yk16203) (Fig. 3d).

The granite is composed of plagioclase (35%–45%), K-feldspar (15%–20%), quartz (15%–20%), biotite (5%–10%), hornblende (5%), and accessory zircon, apatite, titanite, and Fe–Ti oxides (Fig. 3b, c). The granite porphyry has a porphyritic texture, comprising plagioclase, minor K-feldspar, and quartz phenocrysts

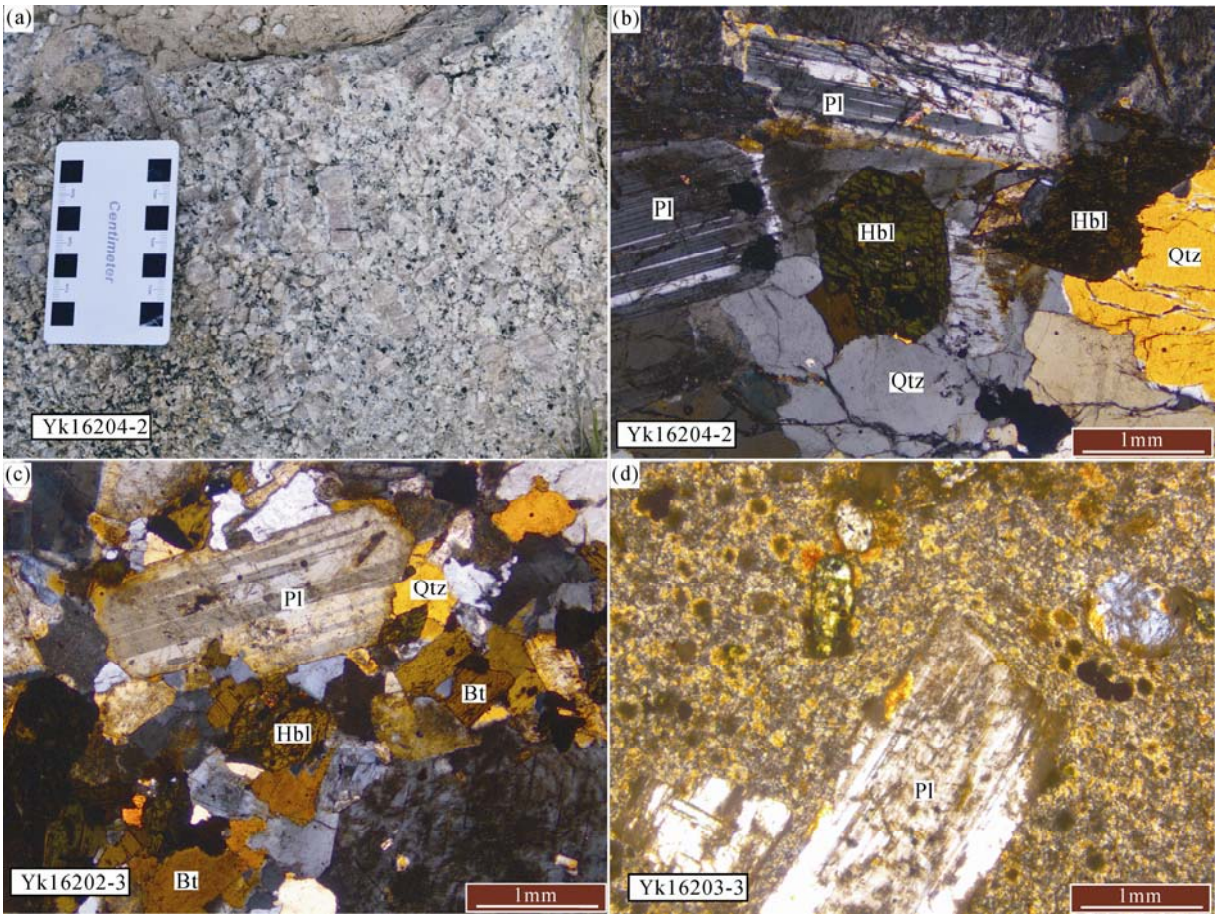

Fig. 3. Field and thin section photographs of the Baleigong Granites.
(a–b) Granitic texture in sample Yk16204–2, showing lath-shaped plagioclase grains, dark green lozenge-shaped prisms of hornblende, and euhedral quartz. (c) granite samples (Yk16202–3) showing a coarse-grained granitic texture. Plagioclase grains are white and lath-shaped, K-feldspar is white and relatively tabular, hornblende is dark green and appears as lozenge-shaped prisms, and quartz is colorless and anhedral. (d) granite porphyry samples (Yk16203–3) showing coarse-grained porphyritic and spherulitic textures. Plagioclase phenocrysts show evidence for dissolution, and the groundmass shows spherulitic texture. f: Abbreviations: Hbl: Hornblende; Pl: Plagioclase; Kfs: K-feldspar; Bt: Biotite; Qtz: Quartz

(15%–20% of the total rock mass) in a matrix (80%–85%) of fine-grained felsic minerals and biotite. The biotite locally shows a spheroidal structure with partial alteration to chlorite (Fig. 3d).

3.2 Analytical methods

3.2.1 Major and trace element analyses

Whole-rock major and trace element compositions were determined at the National Research Center of Geoanalysis, Beijing, China. Major elements were determined using a Philips X-ray fluorescence spectrometer (XRF; PW4400), following the procedures of Norrish and Hutton (1969). The FeO content was determined by a wet chemical method. Trace elements were determined with a Thermofisher ICAP Qc ICP–MS at the IGGE, using procedures similar to those described by Li (1997). Analytical precision was generally better than 5%.

3.2.2 Zircon U–Pb isotope analysis

Zircon grains were separated from a ~3 kg fresh sample using conventional heavy liquid and magnetic separation techniques at the Langfang Diyan Mineral Separating Limited Company (Hebei Province, China). Representative zircon grains were hand-picked under a binocular microscope, mounted in epoxy resin, and polished to expose their cores. Zircon grains were then photographed under transmitted and reflected light, and imaged by cathodoluminescence (CL) at the Gaonian Navigation Technology Company (Beijing, China) to examine their external and internal structures.

U-Pb dating analyses of zircon were conducted by LA-ICP-MS at the State Key Laboratory of Ore Deposit Geochemistry, Institute of Geochemistry, Chinese Academy of Sciences, Guiyang, China. Laser sampling was performed using a GeoLas Pro 193 nm ArF excimer laser. An Agilent 7500x ICP–MS instrument was used to acquire ion-signal intensities. Helium was applied as a carrier gas that was mixed with Argon via a T-connector before entering the ICP–MS. Each analysis incorporated a background acquisition of ~30 s (gas blank) followed by 60 s of data acquisition from the sample. The program ICPMSDataCal was used for offline selection and integration of background and analyte signals, and for time-drift correction and quantitative calibration of the trace element and U-Pb analyses (Jackson et al., 2004; Liu

et al., 2010).

Zircon 91500 was used as an external standard for U-Pb dating, and was analyzed twice every 6–8 analyses. The uncertainty of preferred values for the external standard 91500 was propagated to the ultimate results of the samples (Wiedenbeck et al., 1995). Concordia diagrams and weighted mean calculations were made using Isoplot (Ludwig, 2003). Trace element compositions of zircon grains were calibrated against multiple-reference materials (NIST 610, BHVO-2G, BCR-2G, BIR-1G) combined with Si internal standardization.

3.2.3 Mineral electron microprobe

Electron microprobe analysis of amphibole minerals was conducted at the Key Laboratory of Nuclear Resources and Environment (Ministry of Education, East China University of Technology, Nanchang, China). The instrument used was a JXA-8100M electron microprobe with an accelerating voltage of 15 kV, a current of 2×10^{-8}A, and a beam spot diameter of <2 mm.

4 Results

4.1 Geochemical characteristics

Results of the major and trace element compositions of the eight samples from the Baleigong Granites are presented in Tables 1 and 2. The SiO_2, Na_2O, and K_2O contents are 67.68–69.77 wt%, 3.05–3.61 wt%, and 4.61–5.11 wt%, respectively. Al_2O_3, TiO_2 and MgO contents are 13.93–14.76, 0.52–0.62, and 0.79–0.93 wt%, respectively. In the total alkali–silica (TAS) diagram (Fig. 4a; Middlemost, 1994; Irvine and Baragar, 1971), samples fall in the granodiorite and granite fields. Most samples have high K_2O/NaO ratios (1.31–1.55), with A/CNK values of 0.93–1.02. These values correspond to the high-K calc-alkaline and potassium series, with a metaluminous to slightly peraluminous composition (Fig. 4b–f) (Irvine and Baragar, 1971; Peccerillo and Taylor, 1976; Maniar and Piccoli, 1989; Frost et al., 2001).

Granite samples show high total rare earth element (ΣREE) contents (232–268 ppm). In a chondrite-normalized REE diagram, the samples are enriched in light REE (LREE) and depleted in heavy REE (HREE) (Fig. 5a; Table 3; Sun and McDonough, 1989). The ΣLREE and ΣHREE contents are 204–243 ppm and 24–28 ppm, respectively. The chondrite-normalized REE distribution of the Baleigong Granites reveals an enrichment in the LREE, with a negative Eu anomaly (δEu=0.40–0.56) and high values of $(La/Yb)_N$ (7.46–11.78) and $(La/Sm)_N$ (3.50–4.57). A MORB-normalized trace element spidergram shows enrichment in LILE (Rb, K, and Cs) and depletion in HFSE (Nb, Ta, and Ti) (Fig. 5b; Table 3; Sun and McDonough, 1989).

4.2 Zircon LA-ICP-MS U-Pb geochronology

Three representative granite samples (Yk16203-3, Yk16204-1, and Yk16204-3, with the each sampling location shown in Table 2) were selected for zircon U–Pb dating. The separated zircon grains were commonly euhedral and 50–150 μm long, with length:width ratios of 2:1 to 3:1. The Th/U ratio in most of the analyzed zircon grains was >0.4 (0.41–1.11) and they show a strong oscillatory zoning that is typical of a magmatic origin. Few zircon grains have a residual core (Fig. 6) (Hoskin and Black, 2000; Wu and Zheng, 2004). The U-Pb age data are listed in Table 3.

Zircon grains with oscillatory zoning from samples Yk16203-3, Yk16204-1, and Yk16204-3 were selected for $^{206}Pb/^{238}U$ dating (Fig. 6a, c, e). In sample Yk16203-3, 18 ablation spots gave concordant results (within error) with a weighted mean age of 282.3±2.5 Ma (MSWD=0.09). Seventeen analyses of Yk16203-3 yielded a weighted mean age of 281.9±1.9 Ma (MSWD=0.23) and 20 analyses of Yk16204-3 yielded a weighted mean age of 281.1±2.4 Ma (MSWD=0.17). The LA-ICP-MS U-Pb zircon dating results indicate that the age of the Baleigong granites is 282–281 Ma.

4.3 Mineral electron microprobe data

Electron microprobe data of hornblende are listed in Table 4. The Fe^{3+} and H_2O calculation method just followed the description by Ridolfi et al. (2008, 2010). The hornblendes have SiO_2 contents of 42.26 wt%–46.37 wt%, Al_2O_3 contents of 5.74 wt%–8.86 wt%, MgO content of 7.27 wt%–9.25 wt%, CaO contents of 10.62 wt%–12.24 wt%, and FeO contents of 19.65 wt%–22.45 wt%. Based on the classification of Leake et al. (1997), the amphiboles are Fe-rich calcareous amphibole, mainlyferro-edenite

Table 1 Major oxide (wt%) compositions of granitic samples from the Baleigong Granites

No.	SiO_2	TiO_2	Al_2O_3	Fe_2O_3	FeO	MnO	MgO	CaO	Na_2O	K_2O	P_2O_5
YK16203–1	68.83	0.53	14.31	1.52	1.98	0.06	0.79	1.88	3.37	4.73	0.14
YK16203–2	67.72	0.62	14.28	1.45	2.55	0.08	0.91	2.19	3.36	4.65	0.16
YK16203–3	68.07	0.57	14.34	1.32	2.34	0.08	0.84	2.12	3.52	4.62	0.15
YK16203–4	68.04	0.56	14.55	1.14	2.55	0.07	0.81	2.41	3.33	4.61	0.14
YK16203–5	67.68	0.53	13.93	1.42	2.22	0.07	0.79	2.38	3.05	4.65	0.13
YK16203–6	68.27	0.56	14.52	1.41	2.26	0.07	0.81	2.31	3.32	4.71	0.14
YK16204–1	69.02	0.56	14.76	1.59	1.90	0.07	0.93	2.57	3.61	4.81	0.14
YK16204–2	69.77	0.52	14.22	1.61	1.62	0.06	0.81	2.24	3.30	5.11	0.13

No.	TOTAL	LOI	A/CNK	ALK	A/NK	SI	σ	τ	Tfe	FeO*/MgO
YK16203–1	98.14	1.71	1.02	8.10	1.34	5.86	2.54	20.64	3.35	4.24
YK16203–2	97.97	1.53	0.98	8.01	1.35	6.41	2.60	17.61	3.85	4.24
YK16203–3	97.97	1.99	0.98	8.14	1.33	6.03	2.64	18.98	3.53	4.20
YK16203–4	98.21	1.37	0.98	7.94	1.39	5.77	2.52	20.04	3.58	4.41
YK16203–5	96.85	3.08	0.97	7.70	1.39	5.76	2.40	20.53	3.50	4.43
YK16203–6	98.38	1.37	0.98	8.03	1.38	5.78	2.55	20.00	3.53	4.36
YK16204–1	99.96	0.50	0.93	8.42	1.32	6.42	2.72	19.91	3.33	3.58
YK16204–2	99.39	0.38	0.95	8.41	1.30	5.84	2.64	21.00	3.07	3.79

Table 2 Trace element (ppm) composition of granitic samples from the Baleigong Granites

No.	Be	Mn	Co	Ni	Cu	Zn	Ga	Rb	Sr	Mo	Cd	In	Cs	Ba	Tl	Pb	Bi
YK16203–																	
1	3.38	431.00	6.04	2.49	5.89	79.10	20.70	215.00	194.00	0.50	0.11	0.05	4.77	619.00	0.91	35.50	0.43
2	3.79	600.00	7.34	3.13	10.20	74.30	20.60	214.00	212.00	0.80	0.12	0.06	5.42	667.00	0.92	36.90	0.30
3	4.71	602.00	6.17	2.74	5.18	69.40	21.00	234.00	179.00	0.46	0.12	<0.05	5.26	649.00	1.01	28.80	2.00
4	4.39	568.00	7.09	3.18	4.32	63.70	22.40	217.00	264.00	1.50	0.15	<0.05	8.87	730.00	1.06	25.00	0.09
5	4.10	523.00	6.24	2.76	6.16	61.10	20.20	216.00	66.10	0.42	0.12	0.06	7.63	615.00	0.95	23.40	0.10
6	3.89	528.00	6.90	2.70	5.97	65.50	21.30	209.00	248.00	1.28	0.11	<0.05	8.58	684.00	1.06	37.30	0.10
YK16204																	
1	3.94	510.00	6.28	2.92	3.66	60.50	20.60	253.00	172.00	0.45	0.07	0.06	12.70	496.00	1.13	30.80	0.22
2	3.79	452.00	5.87	2.78	4.75	57.70	20.30	261.00	177.00	0.38	<0.05	0.05	12.50	589.00	1.17	33.60	0.31

No.	Th	U	Nb	Ta	Zr	Hf	Ti	W	As	V	La	Ce	Pr	Nd	Sm	Eu	Gd
YK16203–																	
1	23.90	5.42	21.00	1.87	281.00	8.48	3147.00	3.35	16.90	27.30	57.00	106.00	11.90	42.60	8.43	1.32	6.96
2	23.00	5.59	22.70	1.86	276.00	8.08	3694.00	2.99	15.90	33.30	57.40	109.00	12.20	43.90	8.71	1.38	7.36
3	25.30	5.92	22.00	1.90	279.00	8.34	3277.00	3.21	5.30	29.10	61.60	114.00	12.70	44.40	8.70	1.37	7.41
4	24.60	7.07	22.60	1.94	282.00	8.50	3497.00	3.45	2.61	31.10	58.80	112.00	12.50	44.30	8.86	1.49	7.77
5	24.30	4.67	20.50	1.83	281.00	8.50	3094.00	3.05	11.90	28.40	55.60	105.00	11.80	42.10	8.42	1.42	7.23
6	24.00	6.70	21.60	1.85	280.00	8.18	3257.00	3.17	4.97	29.50	57.60	108.00	12.10	43.90	8.47	1.36	7.14
YK16204																	
1	35.20	4.50	20.40	1.99	277.00	8.19	3204.00	2.34	5.65	33.10	46.50	95.10	11.20	41.70	8.57	1.05	7.70
2	26.70	4.16	19.40	1.83	275.00	8.20	3167.00	2.04	7.24	31.80	48.00	99.10	11.10	40.70	8.33	1.08	7.37

No.	Tb	Dy	Ho	Er	Tm	Yb	Lu	Sc	Y	ΣREE	ΣLREE	ΣHREE	ΣLREE/ ΣHREE	δEu	$(La/Yb)_N$	$(La/Sm)_N$	$(Gd/Yb)_N$
YK16203–																	
1	1.13	6.53	1.22	3.66	0.57	3.76	0.54	6.05	34.60	251.62	227.25	24.37	9.32	0.53	10.87	4.37	1.53
2	1.17	6.97	1.31	3.74	0.56	3.70	0.54	7.28	36.50	257.94	232.59	25.35	9.18	0.53	11.13	4.25	1.65
3	1.15	6.79	1.27	3.74	0.57	3.75	0.55	6.72	36.20	268.00	242.77	25.23	9.62	0.52	11.78	4.57	1.63
4	1.21	6.95	1.33	3.82	0.58	3.88	0.58	7.06	37.80	264.07	237.95	26.12	9.11	0.55	10.87	4.28	1.66
5	1.18	6.80	1.31	3.68	0.56	3.68	0.54	6.17	36.00	249.32	224.34	24.98	8.98	0.56	10.84	4.26	1.63
6	1.18	6.67	1.29	3.59	0.57	3.72	0.55	6.43	36.40	256.14	231.43	24.71	9.37	0.53	11.11	4.39	1.59
YK16204																	
1	1.25	7.53	1.46	4.30	0.68	4.47	0.67	6.65	42.40	232.18	204.12	28.06	7.27	0.40	7.46	3.50	1.43
2	1.20	7.19	1.44	4.18	0.65	4.29	0.62	6.28	40.80	235.25	208.31	26.94	7.73	0.42	8.03	3.72	1.42

(except one plot near the boundary between the magnesiohornblende and ferrohornblende field).

5 Discussion

5.1 Petrogenesis

5.1.1 Petrogenetic type: I–type affinity

Loiselle and Wones (1979) first proposed the concept of A-type granite, which has the characteristics of alkali-rich, water-poor and anorogenic granite. The A-type granites have low contents of Al, Sr, Eu, Ba, Ti, and P, and form from partial melting under low-pressure and high-temperature conditions. A-type granites, therefore, are commonly generated during crustal extension or post-collisional crustal thinning (Zhang et al., 2012; Zhang, 2013).

The Baleigong granites consist of alkali-feldspar, plagioclase, quartz, biotite, and minor amphibole. The amphiboles yield $(Ca+Na)_B$ values of 1.8481–1.9913 (i.e., >1.34) and Na_B values of 0.0794–0.1568 (<0.67). These values correspond to Fe-rich calcic amphibole, such as ferro-edenite and ferrohornblende. The lack of alkali amphibole indicates that the Baleigong granites do not belong to A-type granite (Fig. 7) (Liu, 1986; Leake et al., 1997; Gill, 2010; Liu et al., 2015). The existence of melanocratic minerals (e.g., amphibole and biotite), low CaO content (1.88–2.57 wt%) and high K_2O-content (4.61–5.11 wt%) in the granite is indicative of a high-K calc-alkaline, I-type granite.

In granite discrimination diagrams, samples from the Baleigong granites are plotted near the boundary between the I–S- and A-type fields, showing the characteristics of I-type granite (Whalen et al., 1987) (Fig. 8). It is also shown that P_2O_5 decreases with increasing SiO_2, whereas Pb moves in the opposite direction (Fig. 9). This feature further indicates an I–type affinity (Chappell and White, 1992).

The chondrite-normalized REE patterns of the Baleigong granites are enriched in LREE and show a negative Eu anomaly. This differs from the characteristic swallow-shaped REE pattern of A-type granites and further indicates that the Baleigong granites is not an A-type granite (Deng et al., 2016; Wang et al., 2007a; Wang et al., 2013; Zhang et al., 2012; Zhang, 2013). In MORB-normalized trace element spidergrams, the Baleigong granite is enriched in LILE (Rb, K, and Cs) and depleted in HFSE (Nb and Ta), consistent with an I-type granite produced by the remelting of igneous rocks at the base of a magmatic arc (Barbarin, 1999; Deng et al., 2016). Accordingly, we propose that the Baleigong granites are typical of I-type granites, and belong to a high-K calc-alkaline granite (Barbarin, 1999; Deng et al., 2016).

5.1.2 Sources nature and fractional evolution process

The most of the Baleigong granites show a narrow range of SiO_2 (71.9–73.3 wt%), and exhibit the Nb/Ta values of 10.25–12.20 (approximate to the average value of the crust (12.00–13.00), Barth et al., 2000). This may indicate that magmatic rocks were mainly produced by partial melting of middle-lower crustal rocks and small

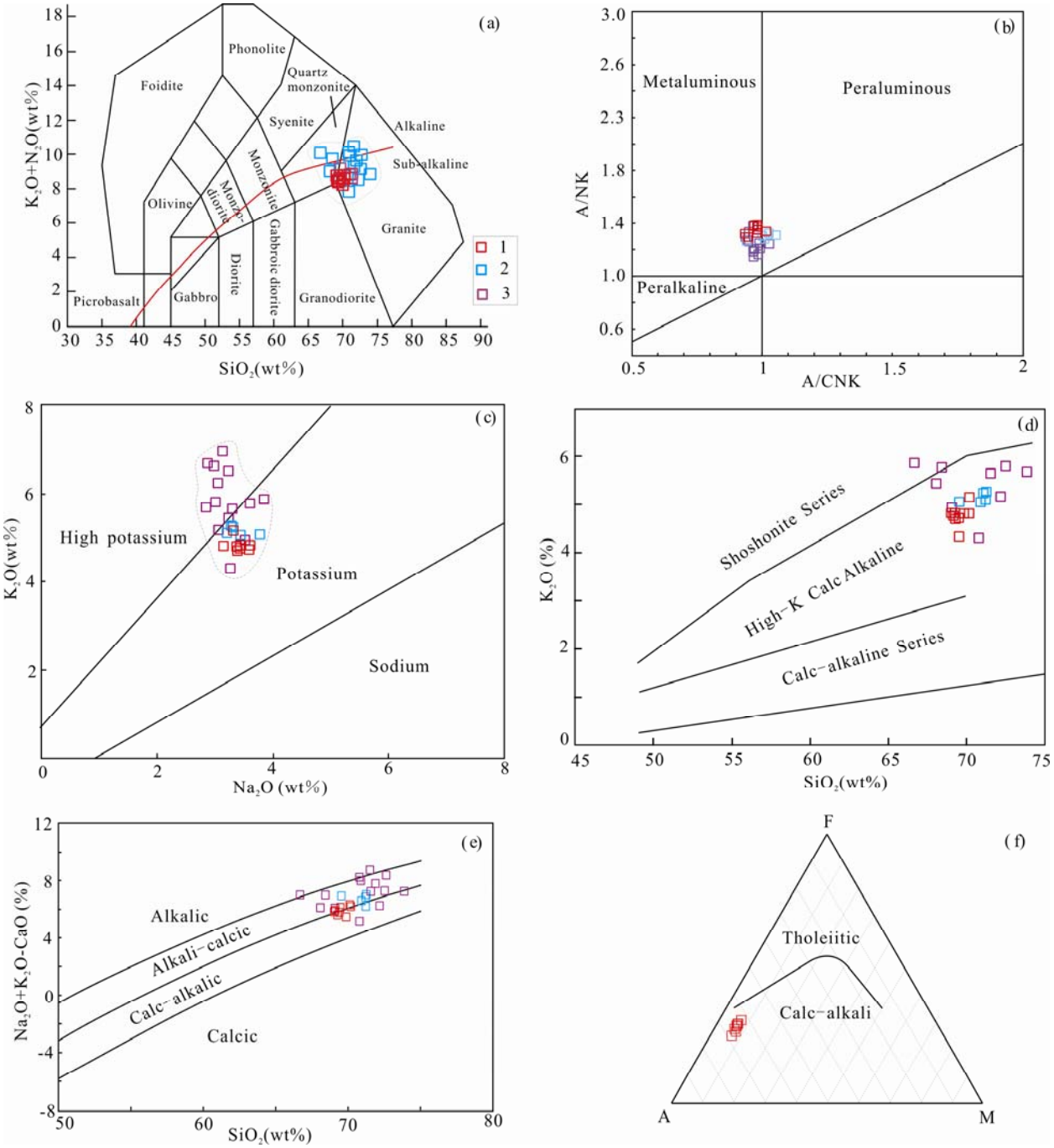

Fig. 4. (a) TAS (Middlemost, 1994; Irvine and Baragar, 1971), (b) A/CNK–A/NK (Maniar and Piccoli, 1989), (c) Na_2O–K_2O (Peccerillo and Taylor, 1976), (d) SiO_2–K_2O (Peccerillo and Taylor, 1976), (e) SiO_2–(Na_2O+K_2O–CaO) (Frost et al., 2001), and (f) AFM (Irvine and Baragar, 1971) diagrams for the Baleigong granites; 1, this study; 2, after Wang et al., 2007a; 3, after Huang et al., 2015.

part of mantle-derived magmas were mixed into the crustal melts during generation of the Baleigong granites (Barbarin, 1990, 1999; Chen and Jahn, 2004; Scaillet et al., 2016). The in situ zircon Hf isotope data (εHf(t) values from –4. 3 to +1.7 and two stage Hf model ages from 1.20 Ga to 1.58 Ga) also indicate that the parental magma was derived mainly from partial melting of Mesoproterozoic amphibolite facies mafic lower crust rocks (Wang et al., 2007a; Huang et al., 2015).

The La/Sm vs. La diagram showing that the magma evolution of the Baleigong granites follow a batch partial melting trend in the early stages, and fractional crystallization probably occurred at shallow depth in the late stages (Fig. 10a) (after Allègre and Minster, 1978). In the late fractional crystallization stages, the fractionation of plagioclase and biotite has played an important role (Fig. 10b–d). This is supported by the depletions in Ba, Sr, Nb, P, Ti and Eu shown in the spidergrams (Fig. 5)

Table 3 LA–ICP–MS U–Pb zircon dating of granitic samples (Yk16203-3, Yk16204-1 and Yk16204-3) from the Baleigong Granites

Sample				Ratios						Age (Ma)					
sport	Th/U	Th	U	$^{207}Pb/^{206}Pb$	1σ	$^{207}Pb/^{235}U$	1σ	$^{206}Pb/^{238}U$	1σ	$^{207}Pb/^{206}Pb$	1σ	$^{206}Pb/^{238}U$	1σ	$^{207}Pb/^{235}U$	1σ
YK16203–3															
1	0.56	204	364	0.05675	0.00225	0.35295	0.01340	0.04530	0.00080	483	89	286	5	307	10
2	0.67	111	166	0.05229	0.00388	0.31665	0.02115	0.04481	0.00089	298	168	283	6	279	16
3	0.61	269	442	0.05104	0.00212	0.31753	0.01390	0.04482	0.00077	243	101	283	5	280	11
4	0.50	209	419	0.05300	0.00181	0.32429	0.01050	0.04442	0.00058	328	78	280	4	285	8
5	0.51	74	145	0.05366	0.00325	0.33114	0.01884	0.04508	0.00072	367	137	284	4	290	14
7	0.65	116	179	0.05913	0.00361	0.36164	0.01757	0.04503	0.00071	572	133	284	4	313	13
8	0.58	103	179	0.05155	0.00270	0.31608	0.01629	0.04477	0.00084	265	125	282	5	279	13
9	0.55	169	310	0.04925	0.00248	0.30070	0.01489	0.04434	0.00078	167	119	280	5	267	12
10	0.58	58	100	0.05265	0.00395	0.32334	0.02431	0.04462	0.00110	322	138	281	7	284	19
11	0.41	200	488	0.05129	0.00187	0.31799	0.01159	0.04473	0.00066	254	88	282	4	280	9
12	0.49	279	575	0.05157	0.00164	0.32458	0.01112	0.04512	0.00069	265	74	284	4	285	9
13	0.56	150	267	0.05504	0.00227	0.34948	0.01568	0.04531	0.00077	413	91	286	5	304	12
15	0.62	114	184	0.05018	0.00407	0.30645	0.02281	0.04440	0.00079	211	–6	280	5	271	18
16	0.74	129	173	0.05251	0.00276	0.32975	0.01823	0.04486	0.00079	309	125	283	5	289	14
17	0.79	126	160	0.05043	0.00265	0.31051	0.01462	0.04476	0.00076	217	122	282	5	275	11
18	0.58	86	149	0.05881	0.00862	0.35610	0.04165	0.04577	0.00144	561	319	289	9	309	31
19	0.58	182	315	0.05190	0.00204	0.32285	0.01268	0.04491	0.00071	280	91	283	4	284	10
20	0.51	45	88	0.05370	0.00415	0.32987	0.02312	0.04470	0.00132	367	176	282	8	289	18
YK16204–1															
1	1.11	199	179	0.05536	0.00334	0.33848	0.01868	0.04472	0.00089	428	140	282	5	296	14
2	0.62	103	167	0.05486	0.00322	0.33688	0.01927	0.04455	0.00095	406	99	281	6	295	15
3	0.60	561	942	0.05274	0.00175	0.33376	0.01153	0.04534	0.00050	317	76	286	3	292	9
4	0.64	407	634	0.05295	0.00169	0.33223	0.01146	0.04503	0.00065	328	72	284	4	291	9
5	0.56	362	647	0.05105	0.00167	0.31503	0.01147	0.04441	0.00080	243	76	280	5	278	9
6	0.57	385	673	0.05443	0.00185	0.33854	0.01267	0.04459	0.00062	387	78	281	4	296	10
7	0.59	466	785	0.05241	0.00143	0.32532	0.00951	0.04482	0.00065	302	63	283	4	286	7
8	0.61	351	578	0.04912	0.00176	0.30261	0.01098	0.04470	0.00069	154	79	282	4	268	9
9	0.58	490	842	0.05269	0.00157	0.32736	0.01013	0.04483	0.00056	322	67	283	3	288	8
10	0.56	353	631	0.05047	0.00162	0.30753	0.00971	0.04427	0.00060	217	81	279	4	272	8
11	0.55	414	749	0.05179	0.00160	0.31909	0.01005	0.04470	0.00058	276	68	282	4	281	8
13	0.64	503	782	0.05215	0.00159	0.32138	0.00999	0.04492	0.00060	300	70	283	4	283	8
14	0.54	211	393	0.04877	0.00190	0.30094	0.01149	0.04487	0.00068	200	95	283	4	267	9
15	0.59	411	696	0.05020	0.00153	0.30930	0.00947	0.04456	0.00053	211	70	281	3	274	7
16	0.64	436	686	0.04987	0.00159	0.30943	0.01175	0.04448	0.00079	191	69	281	5	274	9
18	0.59	610	1025	0.04991	0.00163	0.30542	0.00994	0.04429	0.00061	191	71	279	4	271	8
19	0.67	499	746	0.05774	0.00181	0.35684	0.01168	0.04452	0.00058	520	69	281	4	310	9
YK16204–3															
1	0.63	112	178	0.05102	0.00353	0.31653	0.02526	0.04466	0.00076	243	161	282	5	279	19
2	0.44	352	799	0.04885	0.00153	0.30730	0.01051	0.04514	0.00061	139	74	285	4	272	8
3	0.60	147	246	0.04794	0.00235	0.29587	0.01360	0.04494	0.00083	95	115	283	5	263	11
4	0.50	248	492	0.05136	0.00181	0.31613	0.01149	0.04448	0.00078	257	86	281	5	279	9
5	0.48	93	192	0.05067	0.00290	0.30949	0.01683	0.04467	0.00078	233	133	282	5	274	13
6	0.57	82	143	0.05034	0.00256	0.30819	0.01529	0.04450	0.00078	209	119	281	5	273	12
7	0.66	220	335	0.05120	0.00219	0.31121	0.01255	0.04413	0.00061	250	100	278	4	275	10
8	0.56	76	136	0.04890	0.00314	0.30208	0.01875	0.04512	0.00096	143	144	285	6	268	15
9	0.70	237	338	0.05323	0.00256	0.32985	0.01497	0.04501	0.00071	339	105	284	4	289	11
10	0.59	93	158	0.05401	0.00315	0.32909	0.01751	0.04485	0.00076	372	131	283	5	289	13
11	0.62	147	236	0.05050	0.00310	0.31378	0.01838	0.04504	0.00097	217	138	284	6	277	14
12	0.54	70	129	0.05541	0.00476	0.33442	0.02958	0.04361	0.00115	428	188	275	7	293	23
13	0.61	161	263	0.05192	0.00227	0.32113	0.01458	0.04451	0.00078	283	100	281	5	283	11
14	0.58	146	251	0.05377	0.00264	0.33343	0.01651	0.04475	0.00073	361	111	282	4	292	13
15	0.62	148	238	0.05098	0.00200	0.31335	0.01186	0.04468	0.00071	239	91	282	4	277	9
16	0.60	364	601	0.05182	0.00160	0.32162	0.01120	0.04455	0.00076	276	70	281	5	283	9
17	0.61	242	396	0.05085	0.00185	0.31192	0.01146	0.04441	0.00066	235	85	280	4	276	9
18	0.56	111	198	0.05050	0.00246	0.31019	0.01423	0.04470	0.00072	217	113	282	4	274	11
19	0.45	402	891	0.04975	0.00276	0.30800	0.01641	0.04487	0.00080	183	127	283	5	273	13
20	0.55	110	199	0.04986	0.00269	0.30272	0.01606	0.04435	0.00072	187	126	280	4	269	13

(Barbarin, 1999). Low MgO content in these granites suggests separation of mafic minerals, and petrographic evidence favors a probable fractionation of biotite. Negative Ti anomalies are considered to be related to fractionation of Ti-bearing phases and negative P anomalies should result from apatite separation (Fig. 5b). Strong Eu depletion requires extensive fractionation of plagioclase (Fig. 5a). Accordingly, fractionation of feldspars and biotite has played an important role during the differentiation process.

In the granite discrimination diagram (Fig. 11; Harris et al., 1986), the Baleigong Granites plots in the Volcanic Arc Granite field, possibly indicating that the source area had the characteristics of arc magma. It is therefore speculated that the origin of the Baleigong Granites was mainly associated with partial melting of the thickening

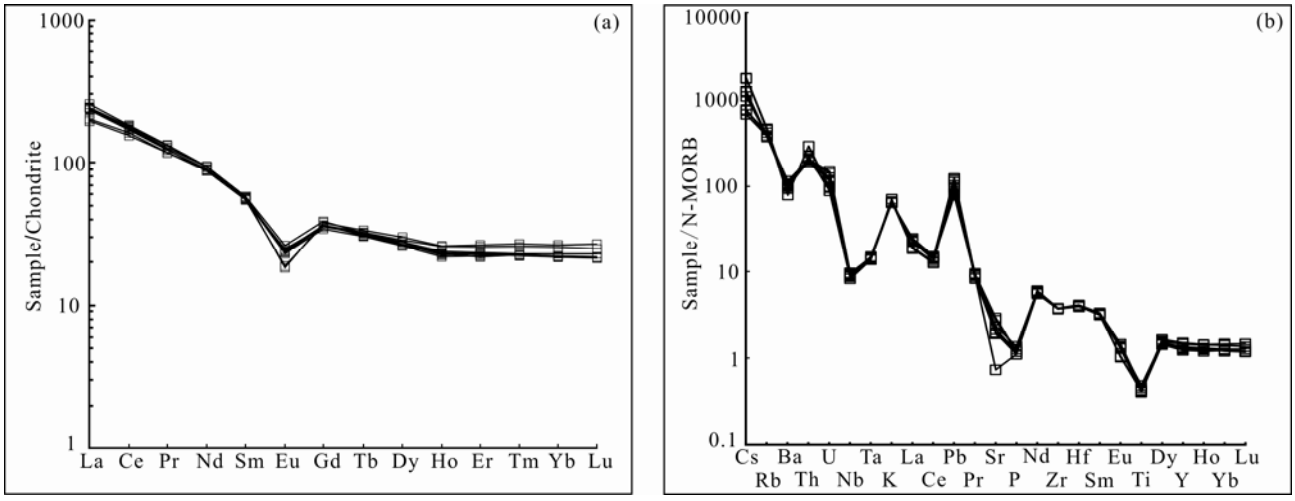

Fig. 5. (a) Chondrite-normalized REE and (b) primitive-mantle-normalized trace element patterns of the Baleigong Granites (normalizing values are from Sun and McDonough, 1989).

Table 4 Electron microprobe analyses of amphiboles from the Baleigong Granites

Sample	YK16202–3	YK16202–4	YK16202–7	YK16204–1	YK16204–2	YK16202–1		
No.	c2	d1	g4	h2–1	n2–1	e1–1	e1–4	e2–3
				Oxide (wt%)				
SiO_2	42.26	42.29	43.39	43.66	43.36	44.99	46.37	44.94
TiO_2	2.25	2.20	2.03	1.75	1.85	1.55	1.08	1.53
Al_2O_3	8.86	8.75	8.22	8.11	8.06	7.01	5.74	6.64
Fe_2O_3	0.00	0.00	0.00	0.00	0.00	0.00	0.00	0.00
FeO	21.47	22.45	21.15	19.65	21.78	21.06	20.27	20.41
MnO	0.42	0.44	0.36	0.65	0.67	0.33	0.50	0.38
MgO	7.64	7.27	8.56	9.25	7.51	8.80	9.11	8.92
CaO	10.70	10.66	10.72	10.62	10.69	10.72	12.24	11.12
Na_2O	1.82	1.80	1.72	1.99	1.87	1.51	1.08	1.50
K_2O	1.18	1.09	1.07	1.08	0.91	0.75	0.51	0.67
F	0.48	0.35	0.31	0.48	0.33	0.16	0.10	0.24
H_2O*	1.71	1.78	1.82	1.74	1.79	1.90	1.91	1.84
Total	99.00	99.40	99.79	99.29	99.06	99.23	98.96	98.43
				Cation proportions per 23 oxygen atoms (Holland and Blundy, 1994)				
Si	6.5670	6.5828	6.6778	6.7026	6.7339	6.9263	7.1047	6.9471
Al^{IV}	1.4330	1.4172	1.3222	1.2974	1.2661	1.0737	0.8953	1.0529
Al^{VI}	0.1896	0.1880	0.1688	0.1699	0.2091	0.1982	0.1412	0.1568
Ti	0.2630	0.2576	0.2350	0.2021	0.2161	0.1795	0.1245	0.1779
Fe^{3+}	0.3682	0.3493	0.3721	0.3530	0.3970	0.4817	0.5614	0.4977
Fe^{2+}	2.4220	2.5732	2.3501	2.1699	2.4318	2.2298	2.0360	2.1409
Mn	0.0553	0.0580	0.0469	0.0845	0.0881	0.0430	0.0649	0.0498
Mg	1.7699	1.6870	1.9639	2.1169	1.7387	2.0197	2.0808	2.0556
Ca	1.7815	1.7779	1.7677	1.7469	1.7788	1.7683	2.0094	1.8418
Na	0.5483	0.5432	0.5132	0.5923	0.5631	0.4507	0.3208	0.4496
K	0.2339	0.2164	0.2101	0.2115	0.1803	0.1473	0.0997	0.1321
Sum	15.6318	15.6507	15.6279	15.6470	15.6030	15.5183	15.4386	15.5023
Si_T*	6.5670	6.5828	6.6778	6.7026	6.7339	6.9263	7.1047	6.9471
Al_T	1.4330	1.4172	1.3222	1.2974	1.2661	1.0737	0.8953	1.0529
Al_C	0.1896	0.1880	0.1688	0.1699	0.2091	0.1982	0.1412	0.1568
$Fe^{3+}{}_C$	0.3682	0.3493	0.3721	0.3530	0.3970	0.4817	0.5614	0.4977
Ti_C	0.2630	0.2576	0.2350	0.2021	0.2161	0.1795	0.1245	0.1779
Mg_C	1.7699	1.6870	1.9639	2.1169	1.7387	2.0197	2.0808	2.0556
$Fe^{2+}{}_C$	2.4093	2.5181	2.2602	2.1580	2.4318	2.1209	2.0360	2.1119
Mn_C	0.0000	0.0000	0.0000	0.0000	0.0073	0.0000	0.0562	0.0000
$Fe^{2+}{}_B$	0.0127	0.0551	0.0899	0.0118	0.0000	0.1089	0.0000	0.0290
Mn_B	0.0553	0.0580	0.0469	0.0845	0.0809	0.0430	0.0087	0.0498
Ca_B	1.7815	1.7779	1.7677	1.7469	1.7788	1.7683	1.9913	1.8418
Na_B	0.1504	0.1090	0.0954	0.1568	0.1403	0.0798	0.0000	0.0794
Ca_A	0.0000	0.0000	0.0000	0.0000	0.0000	0.0000	0.0181	0.0000
Na_A	0.3979	0.4342	0.4178	0.4355	0.4227	0.3710	0.3208	0.3702
K_A	0.2339	0.2164	0.2101	0.2115	0.1803	0.1473	0.0997	0.1321

continental crust, triggered by underplating of the lower crustby basaltic magma (Huang et al., 2015; Wang et al., 2007a). On the Y–Nb, (Y+Nb)–Rb, and Yb–Ta diagrams (Fig. 12; Pearce et al., 1984) the Baleigong granite samples fall in the volcanic arc granite and collisional granite fields, further indicating that the magmatism

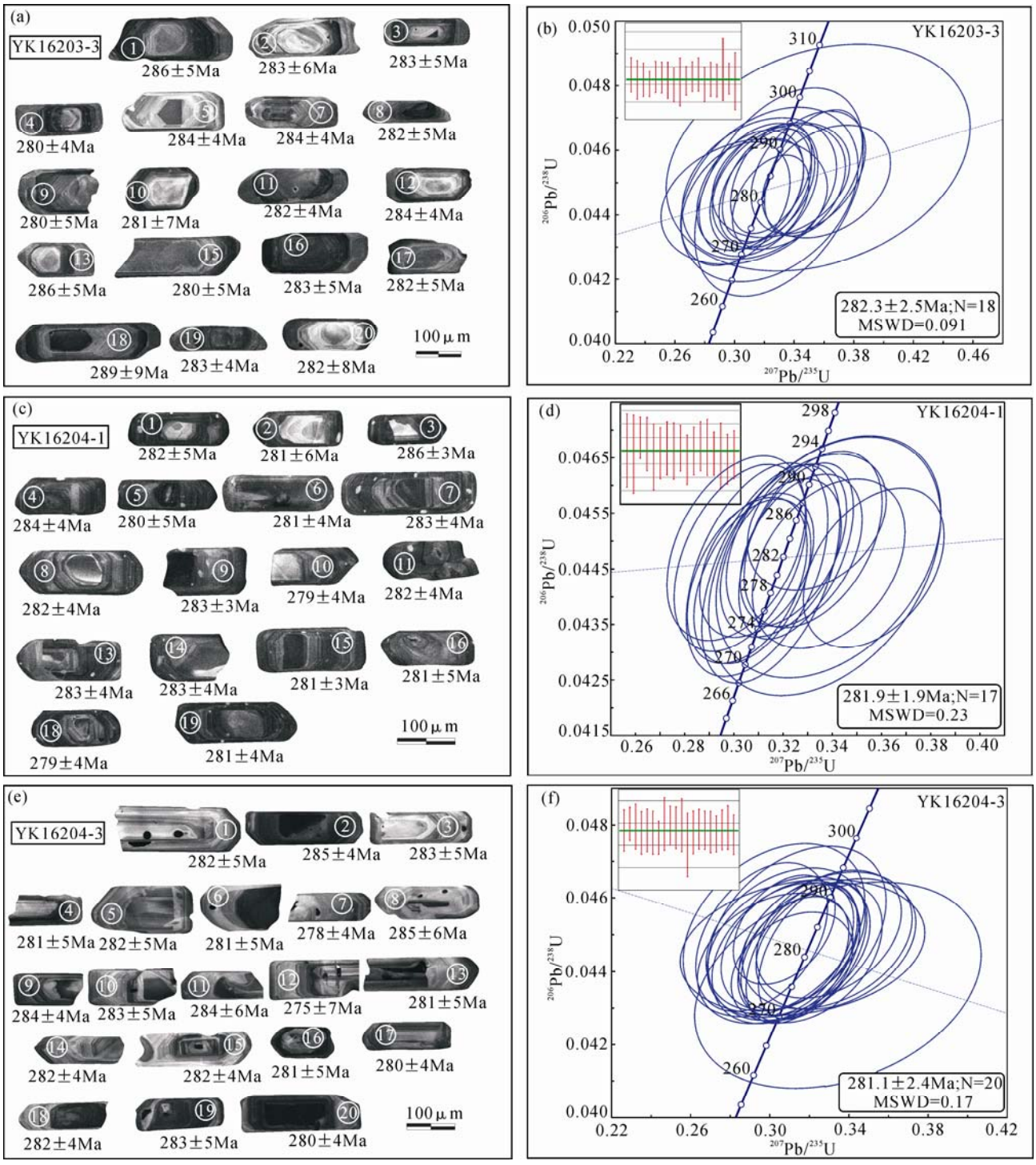

Fig. 6. Representative zircon CL images and concordia diagrams for samples from the Baleigong Granites.
(a, b) Sample YK16203–3; (c, d) sample YK16204–1; (e, f) sample YK16204–3.

originated from remelting of volcanic rocks in a magmatic arc system (Huang et al., 2015; Deng et al., 2016).

5.2 Implications for regional tectonics

The age of the ophiolite and the radiolaria in siliceous rocks in the Southwest Tianshan Orogenic Belt indicate that the Southwest Tianshan Ocean was developed in the early Paleozoic (Li et al., 2002; Wang et al., 2007b; Wang et al., 2012). The subduction of this oceanic crust was dated to 345–331 Ma, based on Sm-Nd and Ar-Ar ages of high-pressure/low-temperature (HP/LT) metamorphic rocks in the West Tianshan Orogenic Belt (Gao et al., 2009a; Li et al., 2016). These results indicate that high-pressure metamorphism associated with subduction occurred at the end of the early Carboniferous (Li et al., 2016).

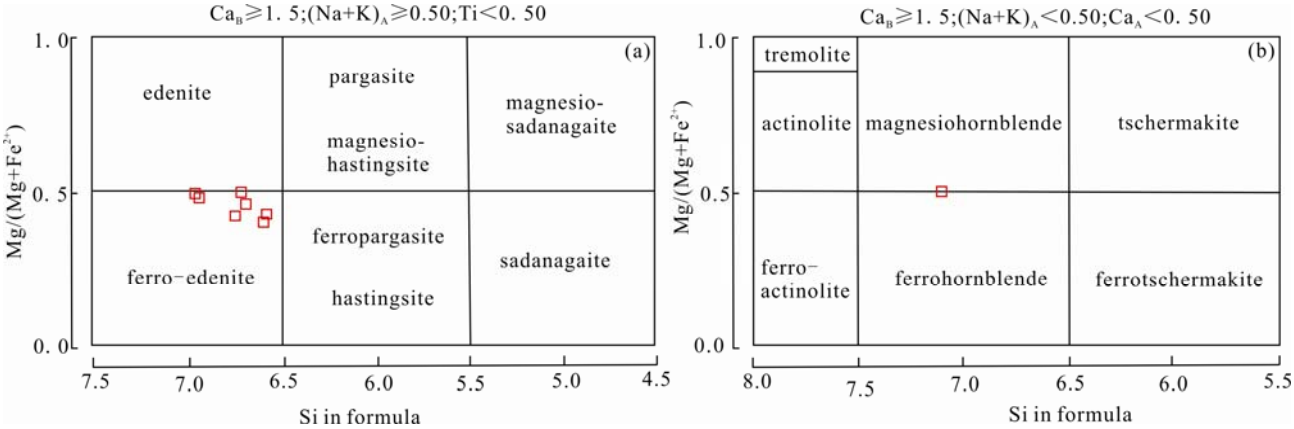

Fig. 7. Amphibole classification diagrams (after Leake et al., 1997) showing the composition of amphiboles from the Baleigong Granites.

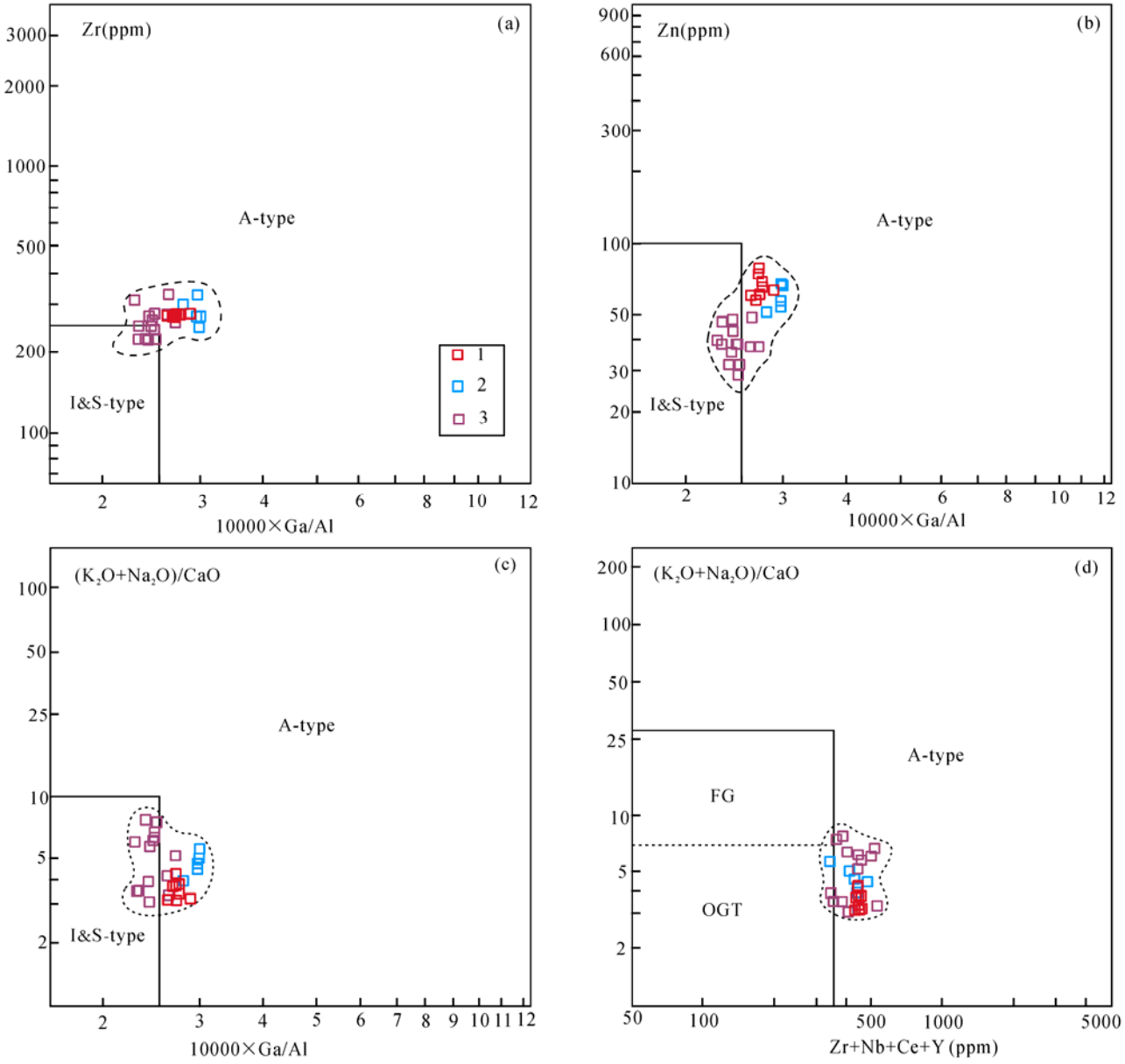

Fig. 8. Granite discrimination diagrams (I-, S-, and A-type; after Whalen et al., 1987).
(a–d) data source: 1, This study; 2, after Wang et al., 2007a; 3, After Huang et al., 2015; Similarly hereinafter. Abbreviations: FG, fractionated felsic granite; OGT, unfractionated M-, I- and S-type granite.

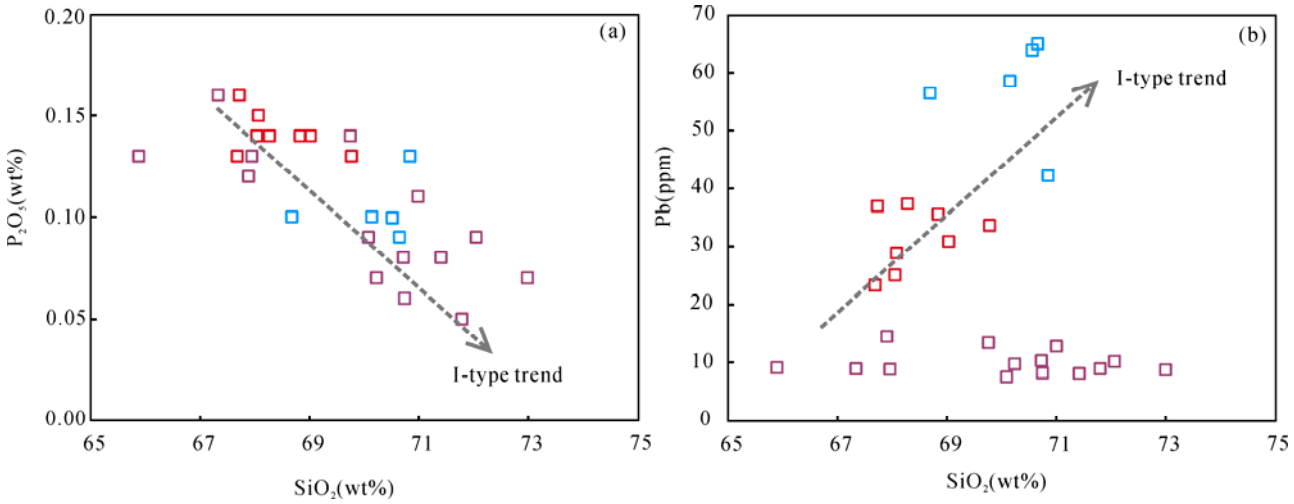

Fig. 9. (a) P_2O_5 vs. SiO_2 and (b) Pb vs. SiO_2 variation diagrams showing that the Baleigong granites follow the trend of I-type proposed by Chappell and White (1992).

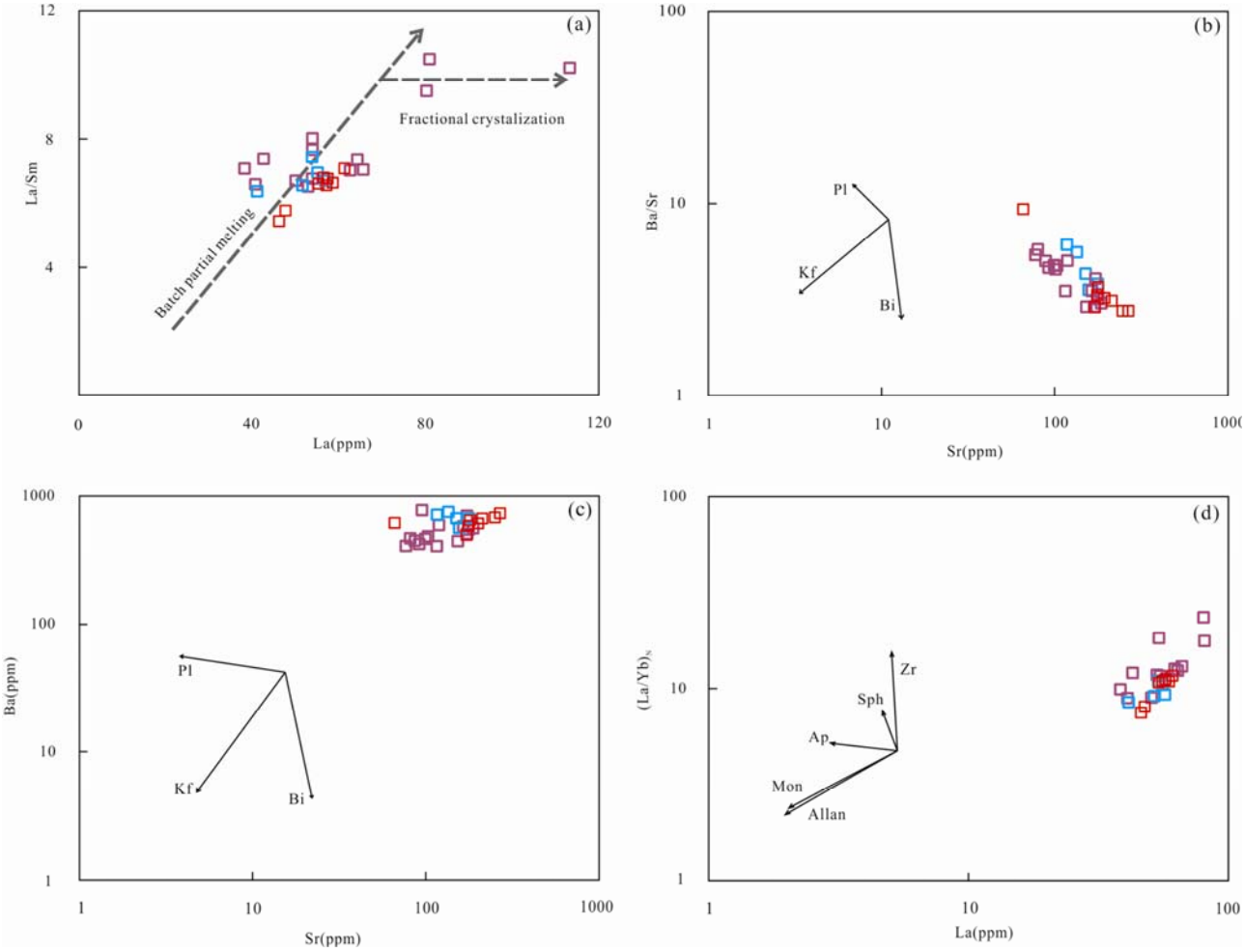

Fig. 10. (a) La/Sm vs. La diagram showing the samples of the Baleigong granites follow a batch partial melting trend, and fractional crystallization probably occurred at shallow depth (after Allègre and Minster, 1978); (b) Ba/Sr vs. Sr and (c) Ba vs. Sr diagrams showing that fractionation of plagioclase plays an important role in the magma differentiation of the Baleigong granites, Partition coefficients of Sr and Ba are from Hanson (1978); (d) $(La/Yb)_N$ vs. La diagram showing the change of REE patterns by separation of accessory minerals, especially allanite and monazite.

Partition coefficients are from Arth (1976) for apatite, Green and Pearson (1986) for sphene (titanite), Mahood and Hildreth (1983) for zircon, Green et al. (1989) for allanite and Yurimoto et al. (1990) for monazite. Abbreviations: Pl, plagioclase; Kf, K-feldspar; Bi, biotite; Zr, zircon; Sph, sphene; Ap, apatite; Mon, monazite; Allan, allanite.

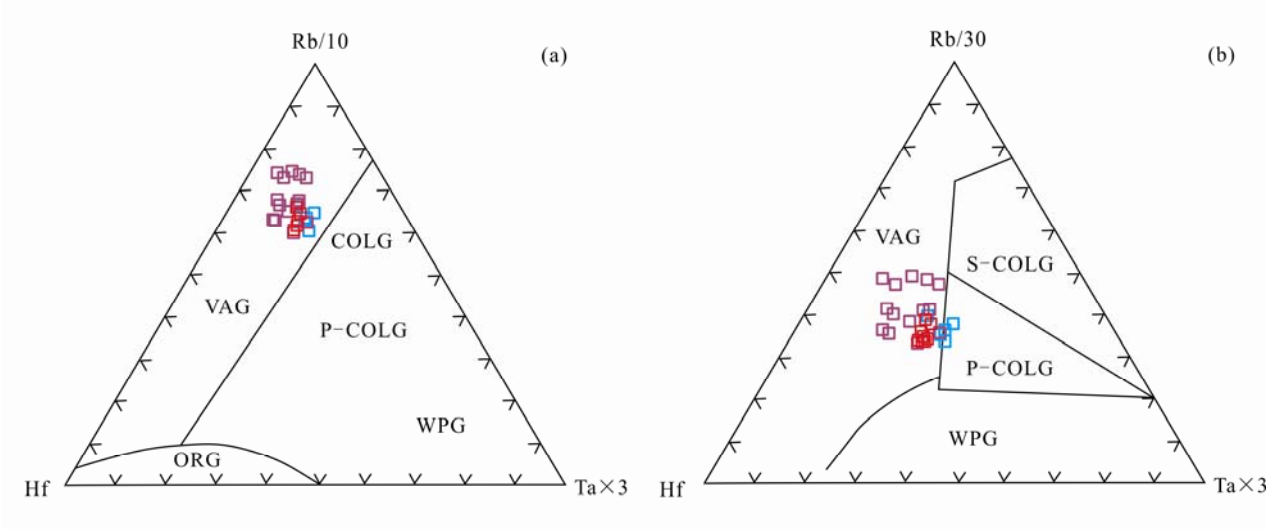

Fig. 11. (a) Rb/10–Hf–Ta×3 and (b) Rb/30–Hf–Ta×3 (Harris et al., 1986) tectonic discrimination diagrams for the Baleigong Granites. Abbreviations: VAG, volcanic arc granite; WPG, within-plate granite; ORG, oceanic ridge granite; COLG, collisional granite; S-COLG, syn-collisional granite; P-COLG, post-collisional granite.

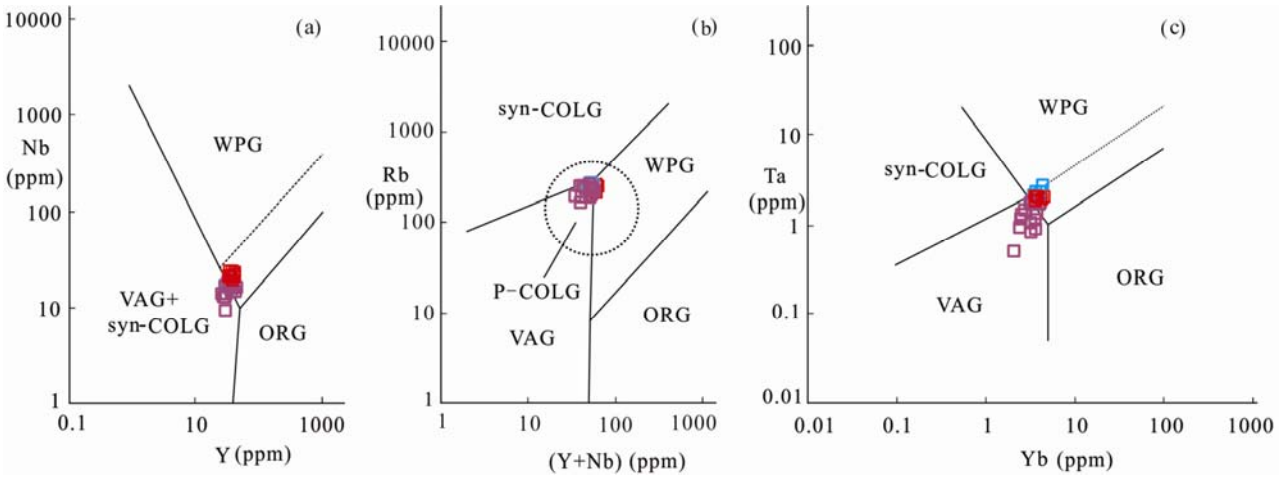

Fig. 12. Geochemical classification diagrams (after Pearce et al., 1984) for the Baleigong Granites. (a) Rb vs. (Yb+Ta) diagram, (b) Rb vs. (Y+Nb) diagram, (c) Nb vs. Y diagram, (d) Ta vs. Yb diagram. Abbreviations: VAG, volcanic arc granite; WPG, within-plate granite; ORG, oceanic ridge granite; COLG, collisional granite; Syn-COLG, syn-collisional granite; P-COLG, post-collisional granite.

The combination of petrologic, structural and geodynamical studies indicates that the high-k calc-alkaline granites are related to continental collision particularly during the post-collisional process (Liègeois et al., 1998; Sylvester, 1998; Barbarin, 1999; Miller et al., 1999; Mo et al., 2007). Remelting of igneous rocks at the base of a magmatic arc likely occurs during the late stage of collision (Wan, 2011; Deng al., 2016). Thus, the emplacement of the Baleigong granites at ~280 Ma indicates that during the early Permian, the Southwest Tianshan was subjected to collisional orogeny following the closure of the South Tianshan Ocean.

The Chuanwulu Alkaline Complex in the western part of the Southwest Tianshan yields a zircon U-Pb age of ~280 Ma (Huang et al., 2010). The geochemical characteristics of the Chuanwulu Alkaline Complex indicate that it was also produced by partial melting of middle and lower continental crust in a post-collisional setting, thereby supporting the proposal that the Southwest Tianshan was subjected to post-collision tectonism during the early Permian (Fig. 13) (Liégeois, 1998; Huang et al., 2010, 2012; Wang et al., 2007a; Deng et al., 2016). Our study indicates that Baleigong granites belong to I-type granite, which was mainly formed in the post-collision stage and represents the late stage of the Orogenic process (Liégeois, 1998; Wang et al., 2007a; Huang et al., 2015).

Based on the above analysis, we suggest that the high-K, calc-alkaline, I-type magmatism that produced the Baleigong granites was directly linked to continental collision. The granites represent post-collisional magmatism in the Southwest Tianshan Orogenic Belt, constrain the timing of collision in the southwestern

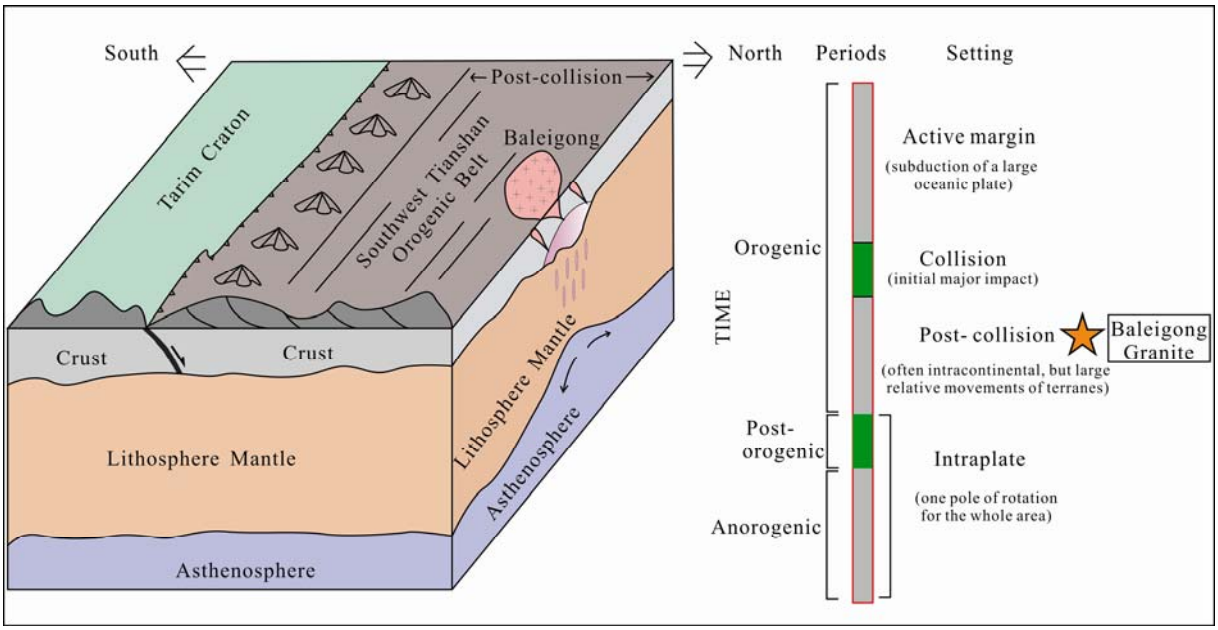

Fig. 13. The cartoon tectonic model of the emplacement of Baleigong Granites (after Liégeois, 1998).

Tianshan, and indicate that the Southwest Tianshan Ocean closed prior to the Permian.

6 Conclusions

(1) The studied Baleigong granite rocks from the Kokshanyan area was emplaced during the Cisuralian (ca. 281–282 Ma).

(2) The geochemical compositions and mineral electron microprobe data indicate that the Baleigong granites are typical of I-type granites, and belong to high-K calc-alkaline granites. The magmatic rocks were mainly produced by partial melting of middle-lower crustal rocks and small part of mantle-derived magmas was mixed into the crustal melts during generation of the Baleigong granites.

(3) The Baleigong granites from the Kokshanyan area may be emplaced in a post-collisional tectonic setting, which was related to the collisional orogeny process following the closure of the South Tianshan Ocean during the Late Paleozoic.

Acknowledgements

This study was financially supported by the National Natural Science Foundation of China (Grant Nos.U1403292, 41472196, 41502085, and 41902214), the National Key Technology Research and Development Program of the Ministry of Science and Technology of China (2015BAB05B04, 2018YFC0604005), and the China Geological Survey Bureau (JYYWF20183702, JYYWF20180602). We are grateful to Prof. Yongjun Di (The China University of Geosciences (Beijing), China) for providing wonderful suggestions for our study. Authors give our sincerest thanks to two anonymous reviewers for their critical and detailed review sand enlightening suggestions that improved the manuscript greatly. We thanks Xiaohu Wang, Jiling Li, Tao Zhang, Ji Ma and Zhilei Ding for assistance during the fieldwork. We are grateful for the laboratory assistance provided by Zhihui Dai at the State Key Laboratory of Ore Deposit Geochemistry, Institute of Geochemistry Chinese Academy of Sciences, Guiyang, China.

Manuscript received May 15, 2019
accepted Aug. 14, 2019
associate EIC XIAO Wenjiao
edited by FEI Hongcai

References

Allègre, C.J., and Minster, J.F., 1978. Quantitative models of trace element behavior in magmatic processes. Earth and Planetary Science Letters, 38(1): 1–25.

Allen, M.B., Windley, B.F., and Zhang, C., 1992. Paleozoic collisional tectonics and magmatism of the Chinese Tien Shan, central Asia. Tectonophysics, 220: 89–115.

Arth, J.G., 1976. Behaviour of trace elements during magmatic processes: a summary of theoretical models and their applications. Journal of Research of the U.S. Geological Survey, 4: 41– 47.

Barbarin, B., 1990. Granitoids: Main petrogenetic classifications in relation to origin and tectonic setting. Geological Journal, 25(3–4): 227–238.

Barbarin, B., 1999. A review of the relationships between granitoid types, their origins and their geodynamic environments. Lithos, 46: 605–626.

Barth, M.G., Mcdonough, W.F., and Rudnick, R.L., 2000. Tracking the budget of Nb and Ta in the continental crust. Chemical Geology, 165(3–4):197–213.

Brunet, M.F., Sobel, E.R., and Mccann, T., 2017. Geological evolution of Central Asian basins and the western Tien Shan range. Geological Society London Special Publications, 427: 1–17.

Cai, K.D., Sun, M., Yuan, C., Zhao, G., Xiao, W.J., Long, X.P., and Wu, F.Y., 2010. Geochronological and geochemical study of mafic dykes from the northwest Chinese Altai: Implications for petrogenesis and tectonic evolution. Gondwana Research, 18(4): 638–652.

Carroll, A.R., Graham, S.A., Hendrix, M.S., Ying, D., and Zhou, D., 1995. Late Paleozoic tectonic amalgamation of NW

China: sedimentary records of the northern Tarim, northwestern Turpan, and southern Junggar basins. Geological Society of America Bulletin, 107(5): 571–594.

Chappell, B.W., and White, A.J.R., 1992. I- and S-type granites in the Lachlan Fold Belt. Transactions of the Royal Society of Edinburgh Earth Sciences, 83(1–2):1–26.

Charvet, J., Shu, L.S., Laurent–Charvet, S., Wang, B., Faure, M., Cluzel, D., Chen, Y., and Jong, K.D., 2011. Palaeozoic tectonic evolution of the Tianshan belt, NW China. Science China Earth Sciences, 54(2): 166–184.

Chen, B., and Jahn, B.M., 2004. Genesis of post-collisional granitoids and basement nature of the Junggar Terrane, NW China: Nd–Sr isotope and trace element evidence. Journal of Asian Earth Sciences, 23(5): 691–703.

Chen, J., Burbank, D.W., Scharer, K.M., Scharer, K.M., Sobel, E., Yin, J.H., Rubin, C., and Zhao, R.B., 2002. Magnetochronology of the upper cenozoic strata in the Southwestern Chinese Tian Shan: Rates of pleistocene folding and thrusting. Earth and Planetary Science Letters, 195(1–2): 113–130.

Chen, Z.L., Wang, Z.X., Han, F.B., Zhang, W.G., Zhang, Q., Zhou, Z.J., Wang, X.H., Xiao, W.F., Han, S.Q., Yu, X.Q., Sun, Y., Nurgazy, T., Latyshev, N., and Zailabidin, H., 2018. Late Cretaceous–Cenozoic uplift, deformation, and erosion of the SW Tianshan Mountains in Kyrgyzstan and Western China. International Geology Review, 60(8): 1–19.

Deng, J.F., Liu, C., Di, Y.J., Feng, Y.F., Su, S.G., Xiao, Q.H., Zhao, G.C., Dai, M., and Duan, P.X., 2016. Crustal convergent and accretional consumption zones, and continent –continent collisional orogenes and subduction–accretional orogenes: Records from the ignerous petrotectonic assemblages. Earth Science Frontiers, 23(6): 34–41 (in Chinese with English abstract).

Frost, B.R., Barnes, C.G., Collins, W.J., Arculus, R.J., Ellis, D.J, and Frost, C.D., 2001. A geochemical classification for granitic rocks. Journal of Petrology, 42(11): 2033–2048.

Green, T.H., and Pearson, N.J., 1986. Rare-earth element partitioning between titanite and coexisting silicate liquid at high pressure and temperature. Chemical Geology, 55(1–2), 105–119.

Gao, J., He, G.Q., Li, M.S., Tang, Y.Q., Xiao, X.C., Zhao, M., and Wang, J., 1995. The mineralogy, petrology, metamorphic PTDt trajectory and exhumation mechanism of blueschists, South Tianshan, northwestern China. Tectonophysics, 250(1–3), 151–168.

Gao, J., He, G.Q., and Li, M.S., 1997. Studies on the features of the structural deformations in the western Tianshan orogenic belt. Acta Geoscientia Sinica, 18: 1–9 (in Chinese with English abstract).

Gao, J., Li, M.S., Xiao, X.C., Tang, Y.Q., and He, G.Q., 1998. Paleozoic tectonic evolution of the Tianshan Orogen, northwestern China. Tectonophysics, 287(1–4):213–231.

Gao, J., and Klemd, R., 2000. Eclogite occurrences in the western Tianshan high–pressure belt, Xinjiang, western China. Gondwana Research, 3(1): 33–38.

Gao, J., Long, L.l., Qian, Q., Huang, D.z., Su, W., and Klemd, R., 2006. South Tianshan: a Late Paleozoic or a Triassic Orogen?. Acta Petrologica Sinica, 22(5):1–13 (in Chinese with English abstract).

Gao, J., Long, L.L., Klemd, R., Qian, Q., Liu, D.Y., Xiong, X.M., Su, W., Liu, W., Wang, Y.T., and Yang, F.Q., 2009a. Tectonic evolution of the South Tianshanorogen and adjacent regions, NW China: geochemical and age constraints of granitoid rocks. International Journal of Earth Sciences, 98(6): 1221–1238.

Gao, J., Qian, Q., Long, L.l., Zhang, X., Li, J.L., and Su, W., 2009b. Accretionary orogenic process of Western Tianshan, China. Geological Bulletin of China, 28(12): 1804–1816 (in Chinese with English abstract).

Gao, J., Klemd, R., Qian, Q., Zhang, X., Li, J.L., Jiang, T., and Yang, Y.Q., 2011. The collision between the Yili and Tarim blocks of the Southwestern Altaids: Geochemical and age constraints of a leucogranite dike crosscutting the HP–LT metamorphic belt in the Chinese Tianshan Orogen. Tectonophysics, 499(1–4): 118–131.

Glorie, S., Grave, J.D., Buslov, M.M., Zhimulev, F.I., Stockli, D.F., Batalev, V.Y., Izmer, A., Van Den Haute, P., Vanhaecke, F., and Elburg, M.A., 2011. Tectonic history of the Kyrgyz South Tien Shan (Atbash-Inylchek) suture zone: The role of inherited structures during deformation-propagation. Tectonics, 30: TC6016.

Gou, L.L., and Zhang, L.F., 2016. Geochronology and petrogenesis of granitoids and associated mafic enclaves from Xiate in Chinese Southwest Tianshan: Implications for early Paleozoic tectonic evolution. Journal of Asian Earth Sciences, 115: 40–61.

Gill, R., 2010. Igneous rocks and processes: a practical guide. Chichester: Wiley– Blackwell, 270–275.

Glorie, S., Grave, J.D., Delvaux, D., Buslov, M.M., Zhimulev, F.I., Vanhaecke, F., Elburg, M.A., and Van den haute, P., 2012. Tectonic history of the Irtysh shear zone (NE Kazakhstan): New constraints from zircon U/Pb dating, apatite fission track dating and palaeostress analysis. Journal of Asian Earth Sciences, 45(4): 138–149.

Glorie, S., Grave, J.D., Buslov, M.M., Zhimulev, F.I., Stockli, D.F., Batalev, V.Y., Izmer, A., Van den haute, P., Vanhaecke, F., and Elburg, M.A., 2015. Tectonic history of the Kyrgyz South Tien Shan (Atbashi–Inylchek) suture zone: The role of inherited structures during deformation–propagation. Tectonics, 30(6): TC6016.

Han, B.F., Guo, Z.J., and He, G.Q., 2010. Timing of major suture zones in North Xinjiang, China: Constraints from stitching plutons. Acta Petrologica Sinica, 26(8): 2233–2246(in Chinese with English abstract).

Han, B.F., He, G.Q., Wang, X.C., and Guo, Z.J., 2011. Late Carboniferous collision between the Tarim and Kazakhstan–Yiliterranes in the western segment of the South Tian Shan Orogen, Central Asia, and implications for the Northern Xinjiang, western China. Earth-science Reviews, 109(3): 74–93.

Han, Y.G., Zhao, G.C., Sun, M., Eizenhöfer, P.R., Hou, W.Z., Zhang, X.R., Liu, D.X., Wang, B., and Zhang, G.W., 2015. Paleozoic accretionaryorogenesis in the Paleo–Asian Ocean: insights from detrital zircons from Silurian to Carboniferous strata at the northwestern margin of the Tarim Craton. Tectonics, 34(2): 334–351.

Han, Y.G., Zhao, G.C., Cawood, P.A., Sun, Min., Eizenhöfer, P.R., Hou, W.Z., Zhang, X.R., and Liu, Q., 2016. Tarim and North China cratons linked to northern Gondwana through switching accretionary tectonics and collisional orogenesis. Geology, 44: 95–98.

Hanson, G.N., 1978. The application of trace elements to the petrogenesis of igneous rocks of granitic composition. Earth and Planetary Science Letters, 38(1): 26– 43.

Hao Jieand Liu Xiaohan, 1993. Ophiolite mélange time and tectonic evolutional model in South Tiansahn area. Sciental Geologica Sinica, 28(1): 93–95(in Chinese with English abstract).

Harris, N.B.W., Pearce, J.A., and Tindle, A.G., 1986. Geochemical characteristics of collision–zone magmatism. *Geological Society London Special Publications*, 19(5): 67–81.

He Guoqi, Li Maosong and Han Banfu, 2001. Geotectonic research of Southwest Tianshan and its west adjacent area, China. Xinjiang Geology, 19:7–11 (in Chinese with English abstract) .

Holland, T., and Blundy, J., 1994. Non-ideal interactions in calcic amphiboles and their bearing on amphibole-plagioclase thermometry. Contributions to Mineralogy and Petrology, 116 (4): 433-447.

Hoskin, P.W.O., and Ireland, T.R., 2000. Rare earth element chemistry of zircon and its use as a provenance indicator. *Geology*, 28(7): 627–630.

Huang, H., Zhang, D.Y., Zhang, Z.C., Zhang, S., Li, H.B., and Xue, C.J., 2010. Petrology and geochemistry of the Chuanwulu alkaline complex in South Tianshan: Constraints on petrogenesis and tectonic setting. Acta Petrologica Sinica, 26(3): 947–962(in Chinese with English abstract).

Huang, H., Zhang, Z.C., Kusky, T., Santosha, M., Zhang, S., Zhang, D.Y., Liu, J.L., and Zhao, Z.D., 2012. Continental

vertical growth in the transitional zone between South Tianshan and Tarim, western Xinjiang, NW China: Insight from the Permian Halajun A_1–type granitic magmatism. Lithos, 55(2): 49–66.
Huang, H., Wang, T., Qin, Q., Tong, Y., Guo, L., Zhang, L., and Hou, J.Y., 2015. Geochronology and zircon Hf isotope of Baleigong granitic pluton in the western part of the South Tianshan Mountains: Petrogenesis and implications for tectonic evolution. Acta Petrologicaet Mineralogica, 34(6): 970–990 (in Chinese with English abstract).
Irvine, T.N., and Baragar, W.R.A., 1971. A guide to the chemical classification of the common volcanic rocks. Canadian Journal of Earth Sciences, 8(5): 523–548.
Jackson, S.E., Pearson, N.J., Griffin, W.L., and Belousova, E.A., 2004. The application of laser ablation–inductively coupled plasma–mass spectrometry to in situ U–Pb zircon geochronology. Chemical Geology, 211(1–2): 47–69.
Jahn, B.M., Wu, B.M., and Chen, B., 2000. Granitoids of the Central Asian Orogenic Belt and continental growth in the Phanerozoic. Transactions of the Royal Society of Edinburgh: Earth Sciences, 91(1–2): 181–193.
Jiang, T., Gao, J., Klemd, R., Qian, Q., Zhang, X., Xiong, X.M., Wang, X.S.,Zhou, T.,and Chen, B.X., 2014. Paleozoic ophiolitic mélanges from the South Tianshan Orogen, NW China: Geological, geochemical and geochronological implications for the geodynamic setting. Tectonophysics, 612–613: 106–127.
Kang, J.L., Zhang, Z.C., Zhang, D.Y., Huang, H., Dong, S.Y., and Zhang, S., 2011. Geochronology and geochemistry of the radiolarian cherts of the Mada'er area, southwestern Tianshan: Implications for depositional environment. Acta Geologica Sinica (English Edition), 85(4): 801–813.
Klemd, R., Hegner, E., Bergmann, H., Pfänderc, J.A., Li, J.L., and Hentschel, F., 2014. Eclogitization of transient crust of the Aktyuz Complex during Late Palaeozoic plate collisions in the Northern Tianshan of Kyrgyzstan. Gondwana Research, 26(3–4): 925–941.
Klemd, R., Gao, J., Li, J.L., and Meyer, M., 2015. Metamorphic evolution of (ultra)–high–pressure subduction–related transient crust in the South Tianshan Orogen (Central Asian Orogenic Belt): Geodynamic implications. Gondwana Research, 28(1): 1–25.
Kröner, A., Windley, B.F., Badarch, G., and Tomurtogoo, O., 2007. Accretionary growth and crust formation in the Central Asian Orogenic Belt and comparison with the Arbian–Nubian shield. Memoir of the Geological Society of America, 200(5): 182–209.
Kröner, A., Kovach, V., Belousova, E., Hegner, E., Armstrong, R., Dolgopolova, A., Seltmann, R., Alexeiev, D.V., Hoffmann, J.E., Wong, J., Sun, Min., Cai, K.D., Wang, T., Tong, Y., Wilde, S.A., Degtyarev, K.E., and Rytsk, E., 2014. Reassessment of continental growth during the accretionary history of the Central Asian Orogenic Belt. Gondwana Research, 25(1): 103–125.
Leake, B.E., Wooley, A.R., Arps, C.E.S., Birch, W.D.,Gilbert, M.C., Grice, J.D., Hawthorne, F.C., Kato, A., Kisch, H.J., Krivovichev, V.G., Linthout, K., Laird, J., Mandarino, J.A., Maresch, W.V., Nickl, E.H., Schumacher, J.C., Smith, D.C., Stephenson, N.C.N., Ungaretti, L., Whittaker, E.J.W., and Guo, Y.Z., 1997. Nomenclature of amphiboles. Report of the subcommittee on amphiboles of the International Mineralogical Association Commission on New Minerals and Mineral Names. The Canadian Mineralogist, 35: 219–246.
Li, X.H., 1997.Geochemistry of the Longsheng Ophiolite from the southern margin of Yangtze Craton, SE China. Geochemical Journal, 31(5): 323–337.
Li, J.L, Gao, J., and Wang, X.S., 2016. A subduction channel model for exhumation of oceanic-type high-pressure to ultrahigh-pressure eclogite-facies metamorphic rocks in SW Tianshan, China. Science China Earth Sciences, 59: 2339–2354.
Li, Y.J., Wang, Z.M., Wu, H.R., Huang, Z.B., Tan, Z.J., and Luo, J.C., 2002. Discovery of radiolarian fossils from the Aiketik Group at the western end of the South Tianshan Mountains of China and its implications. Acta Geologica Sinica (English Edition), 76(2): 146–154.
Li, Y.j., Yang, H.J., Zhao, Y., Luo, J.C., Zheng, D.M., and Liu, Y.L., 2009. Tectonic framework and evolution of South Tianshan, NW China. Geotectonica et Metallogenia, 33(1): 94–104 (in Chinese with English abstract).
Liégeois, J.P, 1998. Perface: Some words on the post-collisional magmatism. Lithos, 45: XV-XVII.
Liu, B.P., Wang, Z.Q., and Zhu, H., 1996. Tectonic framework and evolution of Southwest Tianshan. Beijing: China University of Geosciences Press, 1–56 (in Chinese).
Liu, B., Chen, Z.L., Ren, R., Han, B.F., and Su, L., 2013. Timing of the South Tianshan suture zone: New evidence of zircon ages from thegranitic plutons in Kokshal area. Geological Bulletin of China, 32(9): 1371–1384 (in Chinese with English abstract).
Liu, J.H., 1986. Genetic classification of hornblendes and its application. Journal of Changchun University of Geology, (1): 41–48 (in Chinese with English abstract).
Liu, X.F., Wang, L., Li, H., Liu, J., Zhao, F.F., Lu, Q.X., and Hu, L., 2015. Systematic mineralogical classifications and nomenclatures ofamphibole and pyroxene group minerals. Acta Mieralogica Sinica, 35(1): 19–28 (in Chinese with English abstract).
Liu, Y.S., Hu, Z.C., Zong, K.Q., Gao, C.G., Gao, S., Xu, J., and Chen, H.L., 2010. Reappraisement and refinement of zircon U–Pb isotope and trace element analyses by LA–ICP–MS. Chinese Science Bulletin, 55(15): 1535–1546.
Loiselle, M.C., and Wones, D.R., 1979. Characteristics and origin of anorogenic granites. Geological Society of America, Abstracts with Programs, 11, 468.
Long, X.P., Sun, M., Yuan, C., Xiao, W.J., Lin, S.F., Wu, F.Y., Xia, X.P., and Cai, K.D., 2007. Detrital zircon age and Hf isotopic studies for metasedimentary rocks from the Chinese Altai: Implications for the Early Paleozoic tectonic evolution of the Central Asian Orogenic Belt. Tectonics, 26(5): TC5015.
Long, X.P., and Huang, Z.Y., 2017. Tectonic affinities of microcontinents in the Central Asian Orogenic Belt: A case study of the Chinese Tianshan Orogenic Belt. Bulletin of Mineralogy, Petrology and Geochemistry, 36(5): 771–785 (in Chinese with English abstract).
Ludwig, K.R., 2003. User's Manual for Isoplot 3.00. A geochronological Toolkit for Microsoft Excel. Berkeley Geochronological Center Special Publication, No. 4a.
Mahood, G., and Hildreth, W., 1983. Large partition coefficients for trace elements in high-silica rhyolites. Geochimica et Cosmochimica Acta, 47(1): 11–30.
Maniar, P.D., and Piccoli, P.M., 1989. Tectonic discrimination of granitoids. Geological Society of America Bulletin, 101(5): 635–643.
Middlemost, E.A.K, 1994. Naming materials in the magma/igneous rock System. Earth-Science Reviews, 37: 215–224.
Miller, C., Schuster, R., Klötzli, U., Frank, W., and Purtscheller, F., 1999. Post-collisional potassic and ultrapotassic magmatism in SW Tibet: Geochemical and Sr-Nd-Pb-O isotopic constraints for mantle source characteristics and petrogenesis. Journal of Petrology, 40(9): 1399–1424.
Mo, X.X., Hou, Z.Q., Niu, Y.L., Dong, G.C., Qu, X.M., Zhao, Z.D., and Yang, Z.M., 2007. Mantle contributions to crustal thickening during continental collision; evidence from Cenozoic igneous rocks in southern Tibet. Lithos, 96(1): 225–242.
Norrish, K., and Hutton, J.T., 1969. An accurate X-ray spectrographic method for the analysis of a wide range of geological samples. Geochimica et Cosmochimica Acta, 33(4): 431–453.
Pearce, J.A., Harris, N.B.W., and Tindle, A.G., 1984. Trace element discrimination diagrams for the tectonic interpretation of granitic rocks. Journal of Petrology, 25(4): 956–983.
Peccerillo, A., and Taylor, S.R., 1976. Geochemistry of eocenecalc–alkaline volcanic rocks from the Kastamonu area, Northern Turkey. Contributions to Mineralogy and Petrology, 58(1): 63–81.
Ridolfi, F., Puerini, M., Renzulli, A., Menna, M., and Toulkeridis, T., 2008. The magmatic feeding system of El Reventador volcano (Sub-Andean zone, Ecuador) constrained

by texture, mineralogy and thermobarometry of the 2002 erupted products. Journal of Volcanology and Geothermal Research, 176(1): 94–106.
Ridolfi, F., Renzulli, A., Puerini, M., 2010. Stability and chemical equilibrium of amphibole in calc-alkaline magmas: an overview, new thermobarometric formulations and application to subduction-related volcanoes. Contributions to Mineralogy and Petrology, 160(1): 45–66.
Scaillet, B., Holtz, F., and Pichavant, M., 2016. Experimental constraints on the formation of silicic magmas. Elements, 12: 109–114.
Şengör, A.M.C., Natal'in, B.A., and Burtman, V.S., 1993. Evolution of the Altaid tectonic collage and Palaeozoic crustal growth in Eurasia. Nature, 364(6435): 209–304.
Shu, L.S., Wang, B., and Zhu, W.B., 2007. Age of Radiolarian fossils from the Heiyingshan ophiolitic mélange, Southern Tianshan belt, NW China, and its tectonic significance. Acta Geologica Sinica, 81(9): 1161–1168 (in Chinese with English abstract).
Sun, S.S., and Mcdonough, W.F., 1989. Chemical and isotopic systematics of oceanic basalts: implications for mantle composition and processes. Geological Society London Special Publications, 42(1): 313–345.
Sylvester, P.J., 1998. Post–collisional strongly peraluminous granites. Lithos, 45(1–4): 29–44.
Wan, T.F., 2011. A discussion on the collision time. Earth Science Frontiers, 18(3): 48–56 (in Chinese with English abstract).
Wang, C., Liu, L., Luo, J.H., Che, Z.C., Teng, Z.Z., and Zhang, J.Y., 2007a. Late Paleozoic post–collisional magmatism in the Southwestern Tianshan orogenic belt, take the Baleigong pluton in the Kokshal region as an example. Acta Petrologica Sinica, 23(8): 1830–1840 (in Chinese with English abstract).
Wang, C., Liu, L., Che, Z.C., Luo, J.H., and Zhang, J.Y., 2007b. Geochronology, petrogenesis and significance of Baleigong mafic rocks in Kokshal segment, southwestern Tianshan Mountains. Geological Review, 53(6): 743–754 (in Chinese with English abstract).
Wang, C., Liu, L., Luo, J.H., Che, Z.C., Zhang, J.Y., and Gui, X.J., 2008. Petrogenesis and geological implication of derpentinized peridotites in the Kokshal segment, South Tianshan. Earth Science, 33(2): 165–173 (in Chinese with English abstract).
Wang, Y., Jiao, Y.L., Tong, L.H., and Yao, Y., 2013. The essence of A–type granitoids: A discussion on the opinions held by Prof. Zhang Qi and some other researchers. Acta Petrologica et Mineralogica, 32(2): 260–266 (in Chinese with English abstract).
Wang, Y., Huang, H., Zhang, D.Y., Zhang, Z.C., Encarnacion, J., and Zhao, L., 2012. SHRIMP dating of the Qiqijianake ophiolitic mélange in the Kokshal region, southwestern Tianshan and its tectonic implications. Acta Petrologica Sinica, 28(4): 1273–1281 (in Chinese with English abstract).
Whalen, J.B., Currie, K.L., and Chappell, B.W., 1987. A–type granites: geochemical characteristics, discrimination and petrogenesis. Contributions to Mineralogy and Petrology, 95 (4): 407–419.
Wiedenbeck, M., Alle, P., Corfu, F., Griffin, W.L., Meier, M., Oberli, F., Quadt, A.V., Roddick, J.C., and Spiegel, W., 1995. Three natural zircon standards for U–Th–Pb, Lu–Hf, trace element and REE analyses. Geostandards and Geoanalytical Research, 19(1): 1–23.
Windley, B.F., Allen, M.B., Zhang, C., Zhao, Z.Y., and Wang, G.R., 1990. Paleozoic accretion and Cenozoic redeformation of the Chinese Tien Shan range, central Asia. Geology, 18: 128–131.
Windley, B.F., Alexeiev, D., Xiao, W.J., Kröner, A., and Badarch, G., 2007. Tectonic models for accretion of the Central Asian Orogenic Belt. Journal of the Geological Society, 164(12): 31–47.
Wu, Y.B., and Zheng, Y.F., 2004. Genesis of zircon and its constraints on interpretation of U–Pb age. Chinese Science Bulletin, 49(15): 1554–1569.
Xia, L.Q., Zhang, G.W., Xia, Z.C., Xu, X.Y., Dong, Y.P., and Li, X.M., 2002. Constraints on the timing of opening and closing of the Tianshan Paleozoic oceanic basin: Evidence from Sinian and Carboniferous volcanic rocks. Geological Bulletin of China, 21(2): 55–62 (in Chinese with English abstract).
Xiao, A.C., Jia, C.Z., Yang, S.F., Wei, G.Q., Chen, H.L., and Zhang, C.S., 2000. The kinematics characters of the thrust-fold belts western front regions in Southern Tianshan, China. Acta Sedimentologica Sinica, 18: 439–444 (in Chinese with English abstract).
Xiao, W.J., Shu, L.S., Gao, J., Xiong, X.L., Wang, J.B., Guo, Z.J., Li, J.Y., and Sun, M., 2008. Continental dynamics of the central Asian orogenic belt and its metallogeny. Xinjiang Geology, 26(1): 4–8 (in Chinese with English abstract).
Xiao, W.J., Windley, B.F., Allen, M.B., and Han, C.M., 2013. Paleozoic multiple accretionary and collisional tectonics of the Chinese Tianshan orogenic collage. Gondwana Research, 23(4): 1316–1341.
Xiao, W.J., and Santosh, M., 2014. The western Central Asian Orogenic Belt: A window to accretionary orogenesis and continental growth. Gondwana Research, 25(4): 1429–1444.
Yin, A., Nie, S., Craig, P., Harrison, T.M., Ryerson, F.J., Qian, X.L., and Yang, G., 1998. Late Cenozoic tectonic evolution of the southern Chinese Tian Shan. Tectonics, 17: 1–27.
Yurimoto, H., Duke, E.F., Papike, J.J., and Shearer, C.K., 1990. Are discontinuous chondrite-normalized REE patterns in pegmatitic granite systems the results of monazite fractionation? Geochimica Et Cosmochimica Acta, 54(7): 2141–2145.
Zhang, L.F., Ai, Y.L., Li, Q., Li, X.P., Song, S.G., and Wei, C.J., 2005. The formation and tectonic evolution of UHP metamorphic belt in southwestern Tianshan, Xinjiang. Acta Petrologica Sinica, 21(4): 1029–1038 (in Chinese with English abstract).
Zhang, Q., Ran, H., and Li, C.D., 2012. A–type granite: what is the essence?.Acta Petrologica et Mineralogica, 31(4): 621–626 (in Chinese with English abstract).
Zhang, Q., 2013. The criteria and discrimination for A–type granites: A reply to the question put forward by Wang Yang and some other persons for "A–type granite": what is the essence?. Acta Petrologica et Mineralogica, 32(2): 267–274 (in Chinese with English abstract).
Zhang, Z.C., Dong, S.Y., Huang, H., Ma, L.T., Zhang, D.Y., Zhang, S., and Xue, C.J., 2009. Geology and geochemistry of the Permian intermediate–acid intrusions in the southwestern Tianshan, Xinjiang, China: implications for petrogenesis and tectonics. Geological Bulletin of China, 28(12): 1827–1839 (in Chinese with English abstract).

About the first author

HUO Hailong: male, born in 1988 in Shanxi Province; Ph. D., graduated from Chinese Academy of Geological Sciences. His current research interest focuses on the tectonic evolution of orogenic belts and the deformational processes. Email: huohailong 2012@163.com(H. Huo).

About the corresponding author

CHEN Zhengle, male; born in 1967 in Wenzhou City, Zhejiang Province; doctor advisor; graduated from Peking University. He is now interested in tectonic process of the Tianshan Orogenic Belt, including subduction, collision, and the orogenic collapse. Email: chenzhengle@263.net (Z. Chen).